TA350
.I4
101

CLEMSON COLLEGE LIBRARY

JUN 27 1960

CLEMSON, SOUTH CAROLINA

INDUSTRIAL mathematics

INDUSTRIAL MATHEMATICS

THE JOURNAL OF THE INDUSTRIAL MATHEMATICS SOCIETY

EDITED BY

R. R. McHENRY

H. W. MILNES

VOLUME 10, PART 1

THE INDUSTRIAL MATHEMATICS SOCIETY
DETROIT, MICHIGAN

SERIAL
TA350
.I42
V.10, Pt.1

Copyright 1960, by the Industrial Mathematics Society
100 Farnsworth Avenue, Detroit 2, Michigan
Library of Congress Catalog Card Number 53-39635

EDITORIAL STAFF

Managing Editors

R. R. McHenry
H. W. Milnes

Assistant Editors

A. Butterworth
R. Davies
D. Hughson
J. D. Ryan
F. F. Timpner

LITHOPRINTED IN THE UNITED STATES OF AMERICA BY
CUSHING - MALLOY, INC., ANN ARBOR, MICHIGAN, 1960

FOREWORD

The Industrial Mathematics Society is a professional organization whose objective it is to extend the understanding and application of mathematics in industry. Founded early in 1949, it marked the first organized attempt of any group to foster a closer relationship between mathematics and industry.

It promotes the cause of mathematics in industry through monthly meetings at which technical papers are presented, through lectures by nationally prominent scientists and engineers, through panel groups which concentrate in specialized fields of knowledge, and through publication of worthwhile papers in its annual volume.

Membership is open to engineers, scientists, and mathematicians who are concerned with the effective use of mathematics in industry. Annual dues are $5.00 per year including a subscription to the annual volume, *Industrial Mathematics*. Application forms and information may be obtained by writing to the Secretary, Industrial Mathematics Society, 100 Farnsworth, Detroit 2, Michigan.

EXECUTIVE OFFICERS
INDUSTRIAL MATHEMATICS SOCIETY

President, Robert A. Roggenbuck, Ford Motor Co., Engineering Staff
Vice President, Robert Davies, General Motors Corp., Research Laboratories
Secretary, Frances D. Huntington, F. D. Huntington Co.
Treasurer, E. Roderick Craves, General Motor Corp., Engineering Staff

CONTENTS

		Page
1.	Energy Losses of Small Rotors . . . . . Donald J. Kenney	1
2.	A "Chain Block" Experimental Design With an Application in Fuel Testing. . . Kan-chen Peng	15
3.	A Measure of the Optical Quality of Proposed Automobile Windshield Designs . . . . . John R. Gagnon	25
4.	Fuel Injector Design Problem . . . . . Donald F. Zawada	37
5.	Analysis of Spring Installations for Low-Frequency Suspension of Vehicles . . . . . Raymond R. McHenry	49
6.	Design and Calculation of Progressive Compression Springs . . . . . Albert E. Roller	61
7.	Experiences with Highly-Loaded Gearing. . . . . Forest McFarland	71

1

Energy Losses of Small Rotors *

By Donald J. Kenney, Ph.D.
Research Institute
University of Detroit

ABSTRACT

A free body, rotating in empty space, is predicted to lose a small amount of its energy to the rest of the universe. Because of the abstruse mathematics, founded on uncertain cosmological assumptions (flat space, curved space, anisotropic space, etc.) which predict this energy loss, an experimental demonstration would seem desirable. However, a practical difficulty is that real rotors exchange energy with their surroundings for a variety of reasons: radiant heating or cooling, transfer of momentum to gas molecules exerting a frictional torque on the rotor, interaction of the rotor with external electric or magnetic fields, and so forth.

Neglecting astronomical objects, an evaluation is made of the feasibility of reducing known torques to a level where unknown torques may be detected. One unknown torque considered here, is a gravitational radiation by the rotor, causing an energy loss or rotational decay by the rotor. With present instrumentation, certain kinds of gravitational radiations now seem on the verge of detectability.

INTRODUCTION

Save for the frictionless planets, the concept of a free rotor was long considered academic. Real rotors always suffered the overriding effects of bearing friction and chatter. The introduction of the air bearing was a vast improvement, although gas friction still drags heavily on the rotor. During the last twenty-five years, the work of J. W. Beams and his students (1) has produced a technique for suspending a small rotor magnetically in a vacuum. (See Figure 1.) Under ideal conditions, this method provides a frictionless mounting, and small steel balls and cylinders can be spun magnetically to the bursting speed.

*This work was supported in part by U. S. Army Transportation Research Command, Fort Eustis, Virginia.

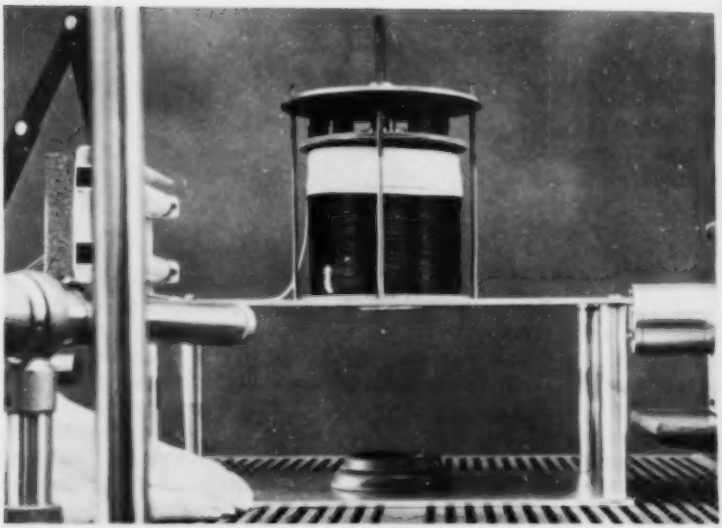

Upon turning off the drive motor (rotating B-field) the rotor will coast freely for many days and transfer its kinectic energy to its surroundings only gradually. It is the manner in which a small steel sphere or cylinder loses its energy that concerns us here.

The kinectic energy of a rotor is of course

$$E = \frac{1}{2} I \omega^2 = \frac{1}{2} I (2\pi f)^2 \tag{1}$$

where I is the moment of inertia and ω and f are the frequencies expressed as radians per second and revolutions per second respectively. The power loss of the rotor is then

$$dE/dt = I \omega \, d\omega/dt = (2\pi)^2 I \, df/dt \tag{2}$$

and

$$\frac{dE/dt}{E} = 2 \frac{d\omega/dt}{\omega} = 2 \frac{df/dt}{f} \tag{3}$$

The factor $\frac{d\omega/dt}{\omega}$ or $\frac{df/dt}{f}$ has the units of reciprocal seconds and is called the "decay ratio." It is a measure of the rotor's deceleration at any frequency and is used throughout this paper,

because of its convenient interchangeability of ω and f. Note that the decay ratio is independent of the shape, mass and hence, moment of inertia of the rotor.

I. Gravitational Radiation

Table 1 outlines the various kinds of g-radiation. The first type ($d\vec{g}/dt \neq 0$) or Cavendish (2) radiation is caused by a time variation of the g-force and is most often characterized as the quadrupole radiation emitted by a rotating dumb-bell. The second type ($d\vec{g}/dt = 0$) is hard to visualize but always seems to be some function of the (v/c) ratio.

Table 1 - Gravitational Radiations

TYPE	TOTAL POSSIBLE POWER RADIATED
FIRST TYPE (Quadrupole)	$k\omega$
SECOND TYPE	
LAPLACE (Doppler Shift)	$k'(\frac{v}{c})E\omega$
BIRKHOFF (Accelerational)	$k''(\frac{v}{c})^3 E\omega$
EINSTEIN (Eddington)	$k'''(\frac{v}{c})^5 E\omega$
GENERAL FORM	$k(\frac{v}{c})^n E\omega$

Laplace radiation (v/c) is a type of gravitational Doppler effect or aberration drag (3). Birkhoff radiation $(v/c)^3$ is conceived to arise because each point mass acts in such a way as to detract from the energy it possesses by virtue of being in an acceleration field (4)(5). Einstein radiation $(v/c)^5$ has been discussed by Eddington (6) who derived the magnitude of its effect on rotating cylinders.

Using Birkhoff radiation, the $(v/c)^3$ type, as an example, we may evaluate the decay ratio, $\frac{d\omega/dt}{\omega}$, for a cylindrical ($k'' = 4.57$) or spherical rotor ($k'' = 3.68$). Since Beams has shown (7) that steel rotors burst at a maximum rim velocity, v, of about 10^5 cm/sec, regardless of size, we may quickly estimate the maximum g-radiation effect for a cylindrical rotor.

$$\frac{d\omega/dt}{\omega} = \frac{1}{2} k''(\frac{v}{c})^3 \omega = \frac{(2.28)(10^5)^3 \omega}{(3 \times 10^{10})^3} \qquad (4)$$

$$\frac{df/dt}{f} = 5.3 \times 10^{-16}(f) \qquad (5)$$

The smallness of this power loss can be emphasized by imagining a megacycle rotor (10^6 revolutions per second) with a decay ratio of the order of 10^{-10} (sec^{-1}). This means the rotor would lose 10^{-4} rev/sec, every second, or would require 10^4 seconds (about 3 hours) to lose one revolution per second.

When the decay ratio for g-radiation is compared to the decay ratio due to other causes (gas friction, etc.), the task of experimentally discriminating out the g-radiation effect seems formidable though not impossible.

It might be well to consider the Laplace type since this would give a more favorable v/c factor than Birkhoff radiation. However, long standing astronomical observations, which have never been challenged, give little support to this aberration drag. For example, it was Laplace himself who showed that observable effects should occur in the motion of the moon-of a kind that are in fact *not* observed - unless c, the speed of gravitation, was at least 100 million times the speed of light (3).

II. Uncertainty in Frequency Measurements

A. Uncertainty Principle

Small changes in rotational frequency might be significant or might be caused by random errors of measurement. In order to rely on frequency changes, it is necessary to explore the precision of frequency measurement and the limits of data refinement.

The ultimate, inherent limitation in any measurement is, of course, the Heisenberg Uncertainty Principle, which leads directly to the concept of quantum states. An object must have a statistical number of quantum levels available to it, before its frequency can be measured with any degree of precision. In the case of a solid cylinder rotating at high speeds, this means the angular momentum should not be allowed to become quantized.

This means that as the radius of the rotor decreases, the frequency must exceed an ever increasing number to obtain a statistical number of quantum states. Estimations quickly show that the effect will not be serious for rotors larger than 10^{-3} cm in diameter.

B. Effect of Light on the Rotor

As a consequence of the Uncertainty Principle, it must be remembered that any attempt to measure rotational velocity too

exactly would result in a disturbance of this velocity by the measuring probe and method of measurement. Presumably, the least disturbance would be caused by a light beam, when the rotational frequency is measured photo-electrically. This disturbance might not be negligible, and it might be well to estimate the effect of light on the rotor.

The effect of light may be subdivided into absorption, transmission (absorption with re-emission), and reflection. These first two effects would disturb the temperature of the rotor, while the last would cause a pressure on the side of the rotor. Let us consider the effect of reflection, first.

1. Light Pressure. In order to measure the frequency of rotation, the photomultiplier tube must receive at least one photon of reflected light from the rotor per revolution. If the efficiency of the tube is one per cent, this means that 100 photons per revolution must be received as a bare minimum. To be safe let us assume that the rotor reflects 1000 photons per revolution. As can be seen from Table 2, this could lead to a fairly intense beam for high frequency rotors.

Table 2 - Light Pressure

Frequency	Light Reflected		Force	Pressure	
(rev/sec)	(photons/sec)	(ergs/sec)	(dynes)	(dynes/cm^2)	(mm Hg)
10^5	10^8	4×10^{-4}	$8/3\times10^{-14}$	3×10^{-13}	2×10^{-16}
10^6	10^9	4×10^{-3}	$8/3\times10^{-13}$	3×10^{-10}	2×10^{-13}
10^7	10^{10}	4×10^{-2}	$8/3\times10^{-12}$	3×10^{-7}	2×10^{-10}
10^8	10^{11}	4×10^{-1}	$8/3\times10^{-11}$	3×10^{-4}	2×10^{-7}
10^9	10^{12}	4	$8/3\times10^{-10}$	3×10^{-1}	2×10^{-4}

It may be seen from Table 2 that this pressure is negligible compared to the vacuum pressure for ordinary rotational frequencies. However, above 10^7 revolutions/sec, light will begin to exert significant pressure and/or friction on the rotor. In other words, we will not be able to measure the rotational velocity without disturbing this velocity. The recovery time of an ordinary photomultiplier tube is about 10^{-7} sec, and this limits the frequency to 10^7 rev/sec anyway.

2. Radiant Heating. If the rotor is something less than a perfect reflector, it will absorb some of the incident light and become warmer. As it becomes warmer, the rotor will begin to radiate more and more energy to the cooler surroundings. This radiation

follows the classical T^4 law. The emissivity coefficient, e, may vary from 0.05 for a very bright surface (such as an iron whisker) to a value of 0.5 for a dull, cast iron finish.

It should be obvious that the rotor will heat up to the temperature where the rate at which it emits energy will approach the rate at which it absorbs energy. This radiative equilibrium temperature may be calculated by using the assumed light reflection values in Table 2. The values for light absorbed are listed in Table 3 and calculated from the relation (6). It should be remembered that higher frequencies require smaller rotors to prevent bursting from centrifugal strain.

$$\text{Light absorbed} = \left(\frac{e}{1-e}\right) \text{(light reflected)} \qquad (6)$$

Table 3 - Radiant Heating

Frequency	Light Reflected	Light Absorbed		Area	T of Rotor*	
(rev/sec)	(ergs/sec)	(e=0.5)	(e=0.05)	(cm^2)	(e=0.5)	(e=0.05)
10^5	4×10^{-4}	4×10^{-4}	2×10^{-5}	4×10^{-1}	Small	Small
10^6	4×10^{-3}	4×10^{-3}	2×10^{-4}	4×10^{-3}	Small	Small
10^7	4×10^{-2}	4×10^{-2}	2×10^{-3}	4×10^{-5}	0.32°C	0.17°C
10^8	4×10^{-1}	4×10^{-1}	2×10^{-2}	4×10^{-7}	156°C	101°C
10^9	4	4	2×10^{-1}	4×10^{-9}	large	large

*The temperature of the surroundings is taken at 27°C.

As can be seen, the rotor will not be heated appreciably until rotational frequencies in excess of 10^7 rev/sec are sought. The rotor will react to this heating by changing its dimensions or moment of inertia, and hence, its rotational velocity. Once again the measuring instrument will disturb the thing it is measuring.

The exact effect of temperature changes on rotational velocity will be discussed in a latter section. For the time being, it might be well to note that 10^7 rps seems to be a practicable limit. For frequencies below this limit, the measuring light beam should be left on continuously so that the rotor may be brought to radiative equilibrium before the critical measurements begin.

III. Gas Friction

It is anticipated that the magnetically suspended rotor will be spun in a vacuum of 10^{-8} to 10^{-10} mm Hg. However, even at these very low pressures there may be sufficient gas to cause a significant frictional drag on the rotor.

When dealing with a high vacuum, it must be remembered that the mean free path of the gas molecules is large. The normal viscosity coefficient, characterizing internal friction of the gas, does not apply. Instead a free-molecule viscosity coefficient, Z, is employed (8). The value of Z is given by

$$Z = P\left(\frac{M.W.}{2\pi R T}\right)^{\frac{1}{2}} \tag{7}$$

where P is the gas pressure; M.W. is the molecular weight; T is the absolute temperature; R is the gas constant. Note that Z, P, M.W., and R are all in c.g.s. units.

The decay ratio for gas friction on a spherical rotor is then

$$\frac{d\omega/dt}{\omega} = \frac{5\ Z}{r\ \rho} \tag{8}$$

where ρ is the density of the rotor. Equation (8) has been verified experimentally by Beams (7).

A range of values for the decay ratio from equation (8) are given in Table 4. It is assumed that a steel sphere ($\rho = 7.8$) is rotating in air at very low pressures and 300° Absolute. By comparing the decay ratio caused by gas friction to that caused by other factors, it will be seen later that gas pressures will have to approach 10^{-10} mm Hg before frictional drag becomes negligible.

Table 4 - Decay Ratio Due to Gas Friction on Spherical Rotors

Pressure	Radius 1	10^{-1}	10^{-2}	10^{-3}
(mm Hg)	r(cm)			
10^{-5}	1.16×10^{-7}	1.16×10^{-6}	1.16×10^{-5}	1.16×10^{-4}
10^{-6}	10^{-8}	10^{-7}	10^{-6}	10^{-5}
10^{-7}	10^{-9}	10^{-8}	10^{-7}	10^{-6}
10^{-8}	10^{-10}	10^{-9}	10^{-8}	10^{-7}
10^{-9}	10^{-11}	10^{-10}	10^{-9}	10^{-8}
10^{-10}	10^{-12}	10^{-11}	10^{-10}	10^{-9}

IV. Rotation of the Earth

The following axioms may be observed:

1. The axis of spin of the rotor (gyro) tends to be vertical due to gravitational attraction. It seems the point of support of such a rotor would logically be above the center of gravity, since the lines of magnetic flux diverge from the bottom of the supporting solenoid.

2. Assume the direction of spin is counterclockwise looking down from above the rotor.

3. An applied external moment cannot change the rate of spin of the rotor or flywheel; it increases the angular momentum of the mounted wheel and ring by making it precess about the vertical axis (9).

4. A spinning gyro tends to maintain its direction fixed in space. Hence, the rotation of the earth produces a forced precession about the precession axis, which is a vector parallel to the axis of rotation of the earth passing through the center of support of the rotor.

5. This enforced precession calls forth a *gyroscopic reaction moment* that is equal and opposite to the external moment that would be required to produce the forced precession.

The rotation of the earth influences rotational decay only in an indirect fashion. A forced precession is elicited in the rotor, which adds or subtracts less than one revolution per day on the absolute rotational velocity. However, once the rotor has attained a maximum spin, it is only the time rate of change of this spin that will be measured, and the earth's rotation will be cancelled out.

The force exerted on the rotor by the support coil, causing it to precess, will not be reflected by a gain or loss in spin. Rather this work done by the coil will be transformed into the kinectic energy of precession, while the spin remains constant.

The earth's rotation does, however, induce a magnetic drag on the rotor. This is because the axis of spin is inclined to the axis of magnetic support due to a gyroscopic reaction moment. The effect of this and other horizontal components of magnetic fields will be considered in the following section.

V. Estimation of Magnetic Drag

By total energy considerations, one may estimate the drag on a cylindrical rotor (radius, r, and length, l) caused by a horizontal magnetic field.

$$\epsilon = v \mathbf{X} B_{(mks)} = r\omega \cos \phi \, B_x \qquad (9)$$

where ϵ is the electric field strength (volts/meter); v is the rim velocity (m/sec); B is the magnetic field strength and B_x is its horizontal component (webers/m^2); where ϕ is the angle of revolution; where $d\phi/dt$ is ω. If J is taken as the current density (amps/m^2) and σ as the conductivity (1/ohm-m), then

$$\text{Power loss} = \int \frac{J^2}{\sigma}\, dV = \int \sigma\, \epsilon^2 dV$$

$$= \int_0^r \int_0^{2\pi} \sigma (r\omega)^2 \cos^2\phi\, B_x^2\, r\, d\phi\, dr \ell \qquad (10)$$

$$\frac{dE/dt}{E} = 2\,\frac{d\omega/dt}{\omega} = \frac{\sigma B_x^2}{\rho}$$

Using appropriate values for the density (kg/m^3) and conductivity of steel and converting webers to gauss

$$\frac{d\omega/dt}{\omega} = 4.27 \times 10^{-6} B_x^2 \qquad \text{(gauss)} \qquad (11)$$

The significance of equation (10) may be realized if it is remembered that the horizontal component of the earth's magnetic field is about 0.2 gauss. Then too, the earth's rotation, as we have seen in the last section, may indirectly cause a horizontal magnetic field component of as much as 3 gauss across the rotor. According to these estimates then, magnetic drag is far from negligible and will have to be carefully considered.

VI. Changes in Temperature

Since metallic rotors will expand or contract with changes in temperature, the law of the conservation of angular momentum would require that this expansion or contraction be accompanied by corresponding changes in angular velocity. If rotational frequencies can be measured to one part in 10^6 or 10^7, then a change in temperature of 1^0 C will make a measurable change in frequency. If a rotor is heated up to 100^0 above room temperature while being driven up to 10^5 rev/sec by the magnetic drive coils, it will gain 240 rev/sec upon cooling to room temperature. Then too, it can be seen from Table 3 that radiant heating by a light beam may slow a small rotor down considerably.

These considerations are not of overwhelming importance because of the lack of a *heat transfer* variable. For example, upon cooling from a higher temperature, the acceleration of the rotor can not be calculated because the cooling rate has not been specified. What is needed is some type of acceleration factor, $d\omega/dt$. In order to evaluate this factor, we must know the heating or cooling rate. If heating or cooling is achieved by radiation only, T^4 law may be used to calculate the energy transfer rate. Table 5 gives a range of decay ratios due to thermal fluctuations for both cylindrical and spherical rotors of various diameters.

Table 5 - Effect of a Thermal Fluctuation of $\pm 1^{\circ}$ C on Decay Ratio

Diameter	Spherical Rotors		Cylindrical*	
(cm)	(e=0.5)	(e=0.05)	(e=0.5)	(e=0.05)
2	6.2×10^{-9}	6.2×10^{-10}	6.5×10^{-9}	6.5×10^{-10}
2×10^{-1}	6.2×10^{-8}	6.2×10^{-9}	6.5×10^{-8}	6.5×10^{-9}
2×10^{-2}	6.2×10^{-7}	6.2×10^{-8}	6.5×10^{-7}	6.5×10^{-8}
2×10^{-3}	6.2×10^{-6}	6.2×10^{-7}	6.5×10^{-6}	6.5×10^{-7}
2×10^{-4}	6.2×10^{-5}	6.2×10^{-6}	6.5×10^{-5}	6.5×10^{-6}

*A constant shape was assumed for the cylinders where $\ell = r\sqrt{3}$.

VII. Elastic Strain

For an estimate of this hoop stress, we may follow Beams and take it approximately equal to $r^2\omega^2$ or N^2. The change in radius may then be calculated from the change in circumference of the rotor, using Q as the circumferential tension.

$$\begin{aligned} \text{Young's Modulus (steel)} &= 2\times10^{+12} \ (\text{dynes/cm}^2) \\ &= Q/[\Delta(2\pi r)/2\pi r] \\ &= Q/(\Delta r/r) \end{aligned} \tag{12}$$

The significance of a variable radius for the rotor is this. Implicitly contained in all that has gone before was the assumption that any power loss of the rotor was accompanied by a decrease in rotational velocity while the radius remained constant. That is

$$dE/dt/E = 2\ d\omega/dt/\omega \tag{13}$$

where E for a cylinder is $\frac{1}{4}\ mr^2\omega^2$.

Now, however, we must write

$$dE/dt/E = 2\ d\omega/dt/\omega + 2\ dr/dt/r \tag{14}$$

since r is also a variable. The problem is to estimate what contribution the r-term in equation (14) will make to the total power loss.

From equation (12) we may write

$$\Delta r/r = \frac{r-r_0}{r} = r^2\omega^2/2\times10^{12} \tag{15}$$

where r_0 is the radius of the rotor at rest. Then

$$\frac{d(r-r_o)}{dt} = \frac{r^3\omega^2}{2 \times 10^{12}} [3\ dr/dt/r + 2\ d\omega/dt/\omega]$$

$$\frac{dr/dt/r}{d\omega/dt/\omega} = \frac{\frac{2\ r^2\omega^2}{2 \times 10^{12}}}{1 - \frac{3\ r^2\omega^2}{2 \times 10^{12}}} = \frac{r^2\omega^2}{10^{12} - 1.5\ r^2\omega^2} \qquad (16)$$

Equation (16), then, gives us the relative contribution of the change in radius of the rotor compared to the change in angular velocity. A range of values are given in Table 6.

Table 6 - Relative Importance of Change in Radius

Radius (cm)	1	10^{-1}	10^{-2}	10^{-3}	10^{-4}
Frequency (rev/sec)					
10^5	9.7×10^{-1}	3.9×10^{-3}	3.9×10^{-5}	3.9×10^{-7}	3.9×10^{-9}
10^6		9.7×10^{-1}	3.9×10^{-3}	3.9×10^{-5}	3.9×10^{-7}
10^7			9.7×10^{-1}	3.9×10^{-3}	3.9×10^{-5}
10^8				9.7×10^{-1}	3.9×10^{-3}
10^9					9.7×10^{-1}

The values recorded are the right hand side of equation 16 and hence, represent the fractional contribution of the change in radius to the power loss. It can be seen that in most cases only a negligible amount of the rotor's energy is stored in mechanical strain. In these cases, we are justified in taking the decay ratio ($d\omega/dt/\omega$) as a measure of the fractional power loss ($dE/dt/E$). However, for larger rotors at higher frequencies, mechanical strain plays an increasingly important part until it eventually comes to equal terms with angular velocity. The blank spaces in Table 6 indicate rim velocities which are well above the bursting strength of known materials.

It would seem then that a rotational frequency of 10^8 (rev/sec) once again represents a natural limit, since for higher values the rotors become vanishingly small. Not only that, if mechanical strain starts to play an important part in power loss, the rotors velocity, shape, and dimensions will have to be measured simultaneously. It would probably be well to do this anyway and be prepared to explain anomalous results. A bulging of rotor at the center would give different results than those predicted here.

VIII. Conclusions

From what has been said above, it may be seen that some of the factors considered may be vital while others may be ignored. Of primary concern is the temperature control of the rotor's surroundings and the production of an ultra-high vacuum in which to spin the rotor. The temperature of the chamber should be controlled $\pm 0.01^{\circ}C$, and gas pressure should be below 1×10^{-10} mm Hg. Both of these conditions are on the fringe of what is now possible to produce in a laboratory.

Factors which are no less critical but more easily nullified are magnetic drag, rotation of the earth, and mechanical vibrations. The last two factors result in a form of magnetic drag. However, there seems to be a good chance of dampening vibrations and controlling stray magnetic fields with a Helmholz coil. Then too, it should be noted that the decay ratio due to g-radiation is a function of angular velocity whereas the magnetic drag decay ratio is not. By going to smaller rotors with higher permissible frequencies, the magnetic drag effect is made less dominant.

Factors which may be controlled by choosing the proper shape, size, strength, and surface condition of the rotor are radiant heating and the stress energy of the rotor. Both of these factors seem to place an upper limit on the rotational frequency of one hundred megacycles. Table 7 gives a comparison of the decay ratios expected from the various factors discussed here.

Table 7

Factors Influencing Megacycle Rotor		
Factor	Condition	Decay Ratio
G-Radiation	10^{6} rps	1×10^{-9}
Gas Friction	10^{-10} mm Hg	1×10^{-10}
Temperature of Surroundings	$\pm 0.1^{\circ}C$.	3×10^{-9}
Light Pressure	1000 photons/rev	$\sim 10^{-13}$ mm Hg
Magnetic Drag	Earth's Field or Tilt of Rotor	$\approx 10^{-6}$
Mechanical Strain	Steel at 10^{6} rps	$< 1\%$ error

Notice that the effect of temperature is cyclic and will cancel out over long periods of time. Hence, even a temperature fluctuation of $\pm 1.0^{\circ}C$ could be tolerated if the rotor is observed over a period

of 24 hours or so. If the light beam, heats the rotor appreciably, it can be left on continuously, as mentioned above, so that the rotor can come to radiative equilibrium with its surroundings.

However, the one irreducible problem that remains is the tilt of the rotor. As explained above, the distance between the magnetic center of support and the center of gravity of the rotor is not known. In lieu of performing the experiment at the north or south pole, a laboratory investigation of center of support and magnetic drag has been inaugurated here and is presently in progress.

REFERENCE

(1) Beams, J. W., *Physics Today*, pp 20-27 (July 1959).
(2) Cavendish, H., *Phil. Trans. Roy. Soc.*, (London) *88* (1798).
(3) Oeuvres de Laplace, Gauthier Villars, pp 326-27, Paris (1880). This Section 22 of Book X of the Mecanique Celeste.
(4) Birkhoff, G. D., "Collected Mathematical Papers," Vol. II, American Math. Soc., New York (1950).
(5) Keith, J. C., *Thesis*, M.I.T. (June 1957). The expression for Birkhoff radiation is contained only implicitly here and in the previous reference. In a forthcoming publication, Keith will explicitly derive the equation for the $(v/c)^3$ effect.
(6) Eddington, A., "Mathematical Theory of Relativity," Cambridge University Press (2nd Edition).
(7) Beams, J. W., *Electronics*, pp 152-55 (March 1954).
(8) Kennard, E. H., "Kinectic Theory of Gases," pp 300-2, McGraw - Hill Book Co., Inc., New York, N. Y. (1938).
(9) Scarborough, J. B., "The Gyroscope, Theory and Applications," pp 37-49, Interscience Publishers, New York, N. Y. (1958).
(10) The exact angle of tilt due to the gyroscopic reaction moment of the rotor is difficult to ascertain because the lever arm must be known, which is the distance between the center of support and the center of gravity of the rotor. Assuming an extreme case of the center of support being at the top of the rotor, we get

$$\text{Sin } \xi = (3.19 \times 10^{-8})\, r\omega = 3.19 \times 10^{-3}$$

where $r\omega$ is the rim velocity (10^5cm/sec) and ξ is the small angle of tilt of the rotors axis from the vertical. Multiplying the support field strength (which could be of the order of 10^3 gauss) by Sin ξ gives the horizontal field component.

2

A "Chain Block" Experimental Design with An Application in Fuel Testing *

By Kan-chen Peng
Research Laboratories
General Motors Corporation

1. INTRODUCTION

An experimenter in the physical sciences often encounters situations in which

(1) The number of "treatments" (or tests) is large and may considerably exceed the size of "block" (such as the length of a day, the capacity of a certain set of test equipment, etc.).
(2) Within the blocks, comparisons are relatively precise.
(3) Elimination of effect due to blocks is desired.

The classical experimental design may fail to meet these conditions successfully. With these needs in mind, Youden and Connor [1] developed the simple chain block designs. Mandel [2] has shown that some of these designs can be generalized so as to adjust for two-way (columns and rows) heterogeneity. This paper discusses the essentials of these designs with an application in fuel testing, and indicates that these designs can be used together with a multiple comparison procedure [3].

2. DESCRIPTION OF THE DESIGN

The principle of the simple chain block design may be illustrated by an example in Table I, for 17 treatments in blocks of 6 or 5 units. The letters denote the treatments. Capital letters refer to treatments having two replications; small letters refer to treatments with a single replication.

The design has a basic linking property. C and D appear both in Blocks 1 and 2, and form the link between these two blocks. E and F, G and H, I and J, and A and B form the links between Blocks 2

*The author is indebted to many people at the Research Laboratories of General Motors Corporation, especially to Dr. F. W. Bowditch for proposing the problem that led to this paper, and to Mr. D. E. Hart and Mr. J. E. Dallemand for encouragement and helpful discussions.

and 3, 3 and 4, 4 and 5, and 5 and 1 respectively. Therefore, the design may be regarded as a chain. The linking property is used to compute the block effects. Each treatment mean is then adjusted for the effects of the block or blocks in which it lies.

TABLE I

A Simple Chain Design for 17 Treatments
in Blocks of 6 or 5

BLOCK

1	2	3	4	5
A	C	E	G	I
B	D	F	H	J
C′	E′	G′	I′	A′
D′	F′	H′	J′	B′
k	l	m	n	o
p	q			

The design is flexible. The basic groups such as A, B may have 1, 2, 3, or more letters (or treatments). However, all groups should have the same number. Additional treatments with a single replication like k, l, m, may be included, subject only to the limitations imposed by the size of block.

The number of error degrees of freedom for a design is

$$N - \nu - b + 1$$

where N is the total number of letters counting replicates, ν the number of letters ignoring replicates, and b the number of blocks. The design in Table I has 6 error degrees of freedom. This number should be checked before adopting a design.

Mandel [2] has shown that some of the simple chain block designs can be generalized in such a fashion that elimination of bias is achieved not only for blocks (columns), but also for another factor, which may, for example, be identified with order within blocks (rows). Table II gives a design with this property for 8 treatments. If the columns are regarded as blocks, this is a typical chain block design, and the chain goes 1, 3, 2, 4, 1.

Again, if the rows are regarded as blocks, the chain goes I, IV, II, III, I. Thus the arrangement is a chain block design for both rows and columns, and treatment means may be corrected to remove the effects of the columns and rows.

TABLE II

A Generalized Chain Block Design

	BLOCKS			
ROWS	1	2	3	4
I	A	B	C	D
II	E	F	G	H
III	G'	H'	B'	A'
IV	C'	D'	F'	E'

Other similar designs are given in Mandel's paper. Note that the number of blocks must be even and that the number of treatments must be a multiple of the number of blocks.

3. BASIC METHOD OF ANALYSIS

An outline of the method of analysis, needed in Section 4, is given here. This follows the presentation developed in [1] and [2].

Let $\alpha_1, \alpha_2, \alpha_3, \ldots, \alpha_v$ denote v treatments, or more generally, groups of treatments with each group having the same number of treatments. Let a_i denote the average yield of group α_i of the first replication, and a'_i denote the average yield of group α_i of the second replication. Then, the general form of a simple chain block design may be shown in Table III. Note that this corresponds to the upper part of Table I.

TABLE III

The General Form of a Simple Chain Block

BLOCK / REPLICATION	1	2	3 . . . . i v
I	a_1	a_2	$a_3 \ldots . a_i \ldots . a_v$
II	a'_2	a'_3	$a'_4 \ldots . a'_{i+1} \ldots a'_1$

Now, define the following relations:

(1) $P_j = a'_{j+1} - a_{j+1}$ (j+1 is interpreted mod v)

(2) $\bar{P} = \frac{\sum P_j}{v}$

(3) G = grand sum = $\sum_{i=1}^{v} a_i + \sum_{i=1}^{v} a_i'$

(4) Sequence S = (v-1), (v-3), (v-5), ..., -(v-5), -(v-3), -(v-1) where S represents an arithmetic progression with common difference -2.

Let e_j (j = 1, 2, ..., v) represent the bias of block j, that is, e_j is the systematic error affecting each yield in block j. If all systematic errors are taken with reference to the overall average, we may impose the restriction,

(5) $\sum_{j=1}^{v} e_j = 0$

Then, to compute $\hat{e}_k$, which is the estimate of an e_k, we permute the P_k cyclically such that P_k is the first term, and write down the P's below S:

S sequence	v-1	v-3	v-5	....	-(v-5)	-(v-3)	-(v-1)
P values	P_k	P_{k+1}	P_{k+2}	....	P_{k-3}	P_{k-2}	P_{k-1}

Now, form the sum of products B_k as follows:

(6) $B_k = (v-1)(P_k - P_{k-1}) + (v-3)(P_{k+1} - P_{k-2})$

$+ (v-5)(P_{k+2} - P_{k-3}) + \ldots$

where the subscripts are interpreted mod v, and finally,

(7) $\hat{e}_k = \frac{1}{2v} B_k$

The recursion formula

(8) $\hat{e}_{k+1} = \hat{e}_k - P_k + \bar{P}$

which can be obtained from (6) and (7) is useful for computing $\hat{e}_2$, $\hat{e}_3$, ..., after $\hat{e}_1$ is computed from (6) and (7).

The analysis of variance is shown in Table IV, as given in [1] and [2], where derivations of least squares solution of the analysis can be found. The analysis for the generalized chain block design follows immediately from the discussions in Section 2 and the formulas given above. Only proper rearrangement of the columns and rows is required. The computed biases for columns and rows, with signs changed, are applied to the original observations as additive corrections.

TABLE IV

Analysis of Variance of Simple Chain Block

Source	Degrees of Freedom	Sum of Squares
Total	$2v - 1$	$S_1 = \sum a_j^2 + \sum a_j'^2 - \frac{G^2}{2v}$
Treatment Ignoring Blocks	$v - 1$	$S_2 = \frac{1}{2} \sum (a_j + a_j')^2 - \frac{G^2}{2v}$
Blocks Eliminating Treatments	$v - 1$	$S_3 = \frac{1}{2} \sum e_j(P_j - P_{j-1})$
Rows	1	$S_4 = \frac{(\sum P_j)^2}{2v}$

4. AN APPLICATION IN FUEL TESTING

A generalized chain block design and a multiple comparison procedure have been successfully applied to a fuel testing problem which was proposed by Fred Bowditch, Fuels and Lubricants Department, General Motors Research.

Briefly, the problem involves testing eight different fuels on a single test engine. Experimental conditions made it necessary to extend the tests over discrete test periods during a day and several days, and it was desired to remove the bias from days and periods. A design as shown in Table II was used for this purpose. A set of 16 measurements from a total of 64 measurements is shown in Table V. These measurements represent crankangle degrees before top dead center (^{0}BTC).

TABLE V

Fuel Testing Measurements (^{0}BTC)
in a Generalized Chain Block

		DAYS 1		2		3		4	
PERIODS	I	(A)	100.78	(B)	97.98	(C)	99.10	(D)	101.78
	II	(E)	105.52	(F)	88.55	(G)	90.95	(H)	109.00
	III	(G')	75.08	(H')	110.65	(B')	112.58	(A')	114.92
	IV	(C')	87.48	(D')	103.60	(F')	88.25	(E')	115.92

After the effects of columns and rows are removed, the differences between the two replications of all fuels are considerably reduced as shown in Table VI.

TABLE VI

Fuel Symbol	Uncorrected		Δ	Corrected		Δ'
A	100.78	114.92	14.14	113.67	110.88	2.79
B	97.98	112.58	14.60	100.57	103.36	2.79
C	99.10	87.48	11.62	96.39	97.41	1.02
D	101.78	103.60	1.82	104.25	103.23	1.02
E	105.52	115.92	10.40	112.64	115.43	2.79
F	88.55	88.25	.30	85.37	82.58	2.79
G	90.95	75.08	15.87	82.47	81.46	1.01
H	109.00	110.65	1.65	105.70	106.73	1.03

TABLE VII

Fuel Testing Measurements

		DAYS					
		1	2	3	4	$\frac{(1)+(2)}{2}$	$\frac{(3)+(4)}{2}$
PERIODS	I	(A) 100.78	(B) 97.98	(C) 99.10	(D) 101.78	(A,B) 99.38	(C,D) 100.44
	II	(E) 105.52	(F) 88.55	(G) 90.95	(H) 109.00	(E,F) 97.04	(G,H) 99.98
	III	(G') 75.08	(H') 110.65	(B') 112.58	(A') 114.92	(G',H') 92.86	(A',B') 113.75
	IV	(C') 87.48	(D') 103.60	(F') 88.25	(E') 115.92	(C',D') 95.54	(E',F') 102.08
$\frac{I+II}{2}$		(A,E) 103.15	(B,F) 93.26	(C,G) 95.02	(D,H) 105.39		
$\frac{III+IV}{2}$		(C',G') 81.28	(D',H') 107.12	(B',F') 100.42	(A',E') 115.42		

This suggests that the design in this case was effective in removing biases. This conclusion is confirmed by the analysis of variance. The detailed procedures for removing biases are shown in Tables VII to X, and the analysis of variance in Table XI. The computations are based on the notations and formulas in Section 3, with rearrangement of rows and columns as indicated in Table VIII and Table IX.

A multiple comparison procedure based on Duncan's method [3] is then used on the 64 corrected measurements to rank the fuels. Note that 6 degrees of freedom are used to correct biases for each of 4 sets of 16 measurements. This fact has to be considered before the multiple comparisons can be made. The application of Duncan's method is rather straightforward. The reader is referred to Duncan's original paper for detailed information of the method.

TABLE VIII

Column Effects

	1	3	2	4	
j	1'	2'	3'	4'	
	(A,E) 103.15 (C',G') 81.28	(C,G) 95.02 (B',F') 100.42	(B,F) 93.26 (D',H') 107.12	(D,H) 105.39 (A',E') 115.42	
P_j	(C',G'-C,G) -13.74	(B',F'-B,F) 7.16	(D',H'-D,H) 1.73	(A',E'-A,E) 12.27	$\overline{P}$ = 1.8550
S	3	1	-1	-3	

$\hat{\gamma}_{1'} = \hat{\gamma}_1 = \frac{1}{8}[3(-13.74) + 1(7.16) - 1(1.73) - 3(12.27)] = -9.0750$

$\hat{\gamma}_{2'} = \hat{\gamma}_3 = -9.0750 - (-13.74) + 1.8550 = 6.5200$

$\hat{\gamma}_{3'} = \hat{\gamma}_2 = 6.5200 - 7.16 + 1.8550 = 1.2150$

$\hat{\gamma}_{4'} = \hat{\gamma}_4 = 1.2150 - 1.73 + 1.8550 = 1.3400$

($\hat{\gamma}_{1'}$ is computed by (7) in Section 3, and the other $\hat{\gamma}_{i'}$'s are computed by (8).)

TABLE IX

Row Effects

	I	III	II	IV	
j	1'	2'	3'	4'	
	(C,D) 100.44 (A,B) 99.38	(A',B') 113.75 (G',H') 92.86	(G,H) 99.98 (E,F) 97.04	(E',F') 102.08 (C',D') 95.54	
P_j	(A,B-A',B') -14.37	(G',H'-G,H) -7.12	(E,F-E',F') -5.04	(C',D'-C,D) -4.90	$\bar{P}$ = -7.8575
S	3	1	-1	-3	

$\hat{\rho}_{1'} = \hat{\rho}_{I} = \frac{1}{8}[3(-14.37) + 1(-7.12) - 1(-5.04) - 3(-4.90)] = -3.8112$

$\hat{\rho}_{2'} = \hat{\rho}_{III} = -3.8112 - (-14.37) - 7.8575 = 2.7013$

$\hat{\rho}_{3'} = \hat{\rho}_{II} = 2.7013 - (-7.12) - 7.8575 = 1.9638$

$\hat{\rho}_{4'} = \hat{\rho}_{IV} = 1.9638 - (-5.04) - 7.8575 = -.8537$

($\hat{\rho}_{1'}$ is computed by (7) in Section 3, and the other $\hat{\gamma}_{i}'$'s are computed by (8).)

TABLE X

Calculation of Corrected Values

		1	2	3	4	1	2	3	4
Correction		+9.08	-1.22	-6.52	-1.34				
I	+3.81	100.78	97.98	99.10	101.78	113.67	100.57	96.39	104.25
II	-1.96	105.52	88.55	90.95	109.00	112.64	85.37	82.47	105.70
III	-2.70	75.08	110.65	112.58	114.92	81.46	106.73	103.36	110.88
IV	+ .85	87.48	103.60	88.25	115.92	97.41	103.23	82.58	115.43

TABLE XI

Analysis of Variance of Fuel Tests

Source	Degrees of Freedom	Sum of Squares	Mean Square	F-Ratio
Total	15	2009.3676	--	--
Fuels	7	1552.234	221.7477	25.117
Columns	3	379.8350	126.6117	14.341
Rows	3	59.6417	19.8806	2.252
Error	2	17.6569	8.8284	--

The sum of squares for Columns is obtained as follows.

$$2\left\{\frac{1}{2}[(-9.0750)(-13.74 - 12.27) + 6.5200(7.16 + 13.74) + 1.2150(1.73 - 7.16) + 1.3400(12.27 - 1.73)]\right\}$$
$$= [236.0408 + 136.2680 - 6.5974 + 14.1236] = 379.8350$$

The sum of squares for Rows is obtained as follows.

$$2\left\{\frac{1}{2}[(-3.8112)(-14.37 + 4.90) + 2.7013(-7.12 + 14.37) + 1.9638(-5.04 + 7.12) - .8537(-4.90 + 5.04)]\right\}$$
$$= 36.0921 + 19.5844 + 4.0847 - .1195 = 59.6417$$

(The factor 2 is used, here and above, because the data in Tables VIII and IX are averages of two original observations.)

The sum of squares for Total is

$$162437.6536 - \frac{(1602.14)^2}{2x8}$$
$$= 162437.6536 - 160428.286 = 2009.3676$$

The sum of squares for Fuels (uncorrected) is

$$161980.520 - 160428.286 = 1552.234$$

REFERENCES

1. Youden, W. J., and Connor, W. S., "The Chain Block Design," *Biometrics*, June 1953, Volume 9, No. 2.
2. Mandel, J., "Chain Block Designs with Two-Way Elimination of Heterogeneity," *Biometrics*, June 1954, Volume 10, No. 2.
3. Duncan, D. B., "Multiple Range and Multiple F Tests," *Biometrics*, March 1955, Volume 11, No. 1.

3

A Measure of the Optical Quality of Proposed Automobile Windshield Designs

By J. R. Gagnon
Systems Engineering Department
Engineering Research and Advanced Product Study Office
Ford Motor Company

ABSTRACT

A measure of the optical quality of automobile windshield designs is obtained by studying the refracting characteristics of the proposed glass surfaces. The deviation of light rays converging to an observation point is calculated for various directions of observation in order to determine deviation patterns that can be analyzed along significant scanning paths.

INTRODUCTION

Conventional optical techniques can be used to determine the refracting characteristics of glass surfaces. However, in studying the optical performance of automobile windshields, it is advantageous to eliminate the need for actual glass models, and work directly with the proposed dimensions. To present the problem and the selected approach for its solution, a schematic of the optical system will be explained.

Figure 1 shows a windshield in the rectangular system of axes X′ Y′ Z′ whose origin O′ is at a point of observation determined by the location of a passenger in the vehicle. From that point, the entire windshield area can be scanned, and the quality of the image seen depends on the particular glass section through which light rays from an object are transmitted.

Consider an arbitrary plane (P), in the environment, containing a vertical linear object ABC. A light ray from point B will meet the outer surface of the windshield at P_1', be refracted to P_1 on the inside surface, and refracted again to O′. As will be shown later, the direction of the ray changes as it passes from one medium to another (air to glass or vice versa), and the resultant effect is that the ray $\overline{P_1 O'}$ appears to come from a point B′ in the plane (P).

Vector $\vec{BB'}$ is defined as the deviation, in plane (P), produced by the windshield, when the direction of observation is $\vec{O'P_i}$.

A similar treatment can be done for a sufficient number of rays coming from the object ABC, and the optical theory will show that the magnitude and direction of the deviation of each ray can be different. Rays from points A and C could appear to come from A' and C' respectively, and the linear object ABC would be perceived by the observer at O' as a curve A'B'C'.

The departure of the image A'B'C' from the actual shape and location of the object ABC is a measure of the optical quality of the windshield when observed along directions $\vec{O'P_i}$. The mathematical development which follows will lead to formulas expressing the deviation vectors as a function of design parameters.

ANALYTICAL DEVELOPMENT

The determination of deviation vectors in a convenient arbitrary plane will be done by computing the direction of light rays in the various optical media present. The law of refraction states that when a ray of light is incident on a surface separating two contiguous homogeneous media, it is refracted in the plane of the incident ray and the normal to the surface at the point of intersection and its direction in that plane is given by

$$\mu_1 \sin \hat{\vec{a}\,\vec{N}} = \mu_2 \sin \hat{\vec{b}\,\vec{N}} \qquad (1)$$

where μ_1 is the index of refraction of the incident medium,

μ_2 is the index of refraction of the refracting medium,

$\hat{\vec{a}\,\vec{N}}$ is the angle between a unit vector $\vec{a}$ in the direction of the incident ray and a unit vector $\vec{N}$ in the direction of the normal, and,

$\hat{\vec{b}\,\vec{N}}$ is the angle between a unit vector $\vec{b}$ in the direction of the refracted ray and the unit vector $\vec{N}$.

To trace a light ray as it passes from one medium to another, it is therefore necessary to know the direction of the incident ray and the direction of the normal to the surface of separation at the point of intersection. The former can be selected, and the latter computed if the equation of the surface is known. To obtain this equation, the coordinates of surface points defining a small section are measured from the proposed windshield design, and used in a surface fitting program based on the method of least squares. The

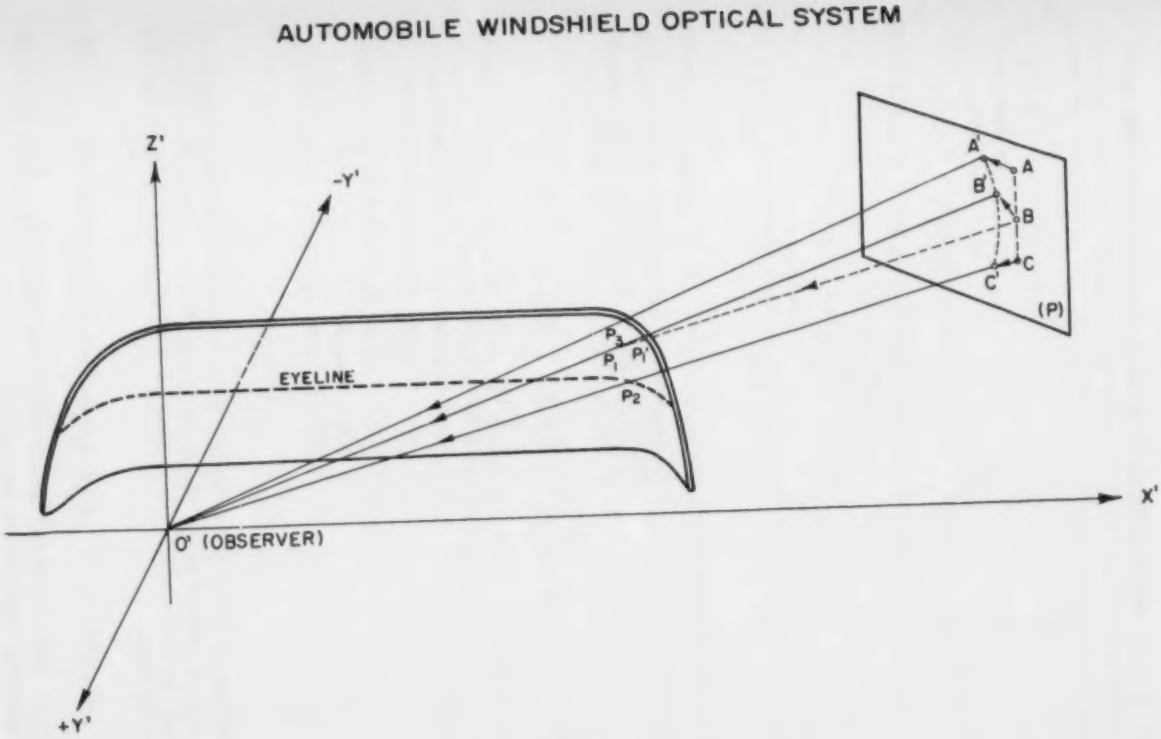
AUTOMOBILE WINDSHIELD OPTICAL SYSTEM
Z'
-Y'
+Y'
X'
EYELINE
O' (OBSERVER)
A'
B'
C'
A
B
C
(P)
P3
P1
P1'
P2

Figure 1

GEOMETRY OF THE RAY-TRACING PROCESS

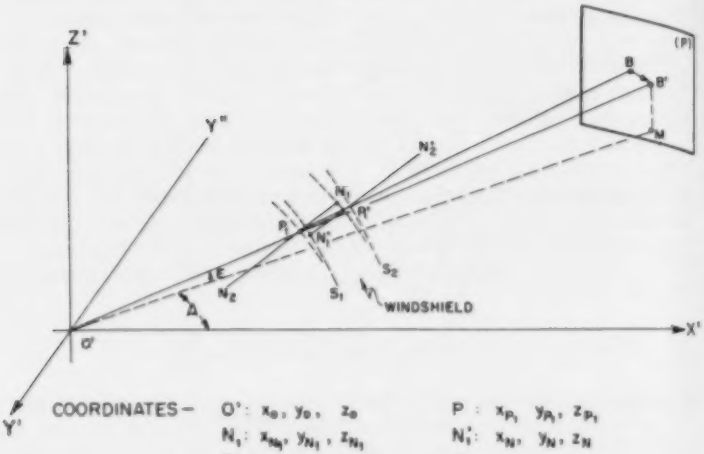

COORDINATES— O': x_0, y_0, z_0 $\quad$ P : $x_{P_1}, y_{P_1}, z_{P_1}$

N_1: $x_{N_1}, y_{N_1}, z_{N_1}$ $\quad$ N_1': x_N, y_N, z_N

P_1': x_P, y_P, z_P $\quad$ B : x_B, y_B, z_B

M : x_M, y_M, z_M $\quad$ B': $x_{B'}, y_{B'}, z_{B'}$

DIRECTION ANGLES— $\overline{O'P_1B'}$ – $\alpha_1, \beta_1, \gamma_1$.

$\overline{N_1P_1N_2}$ – $\alpha_{N_1}, \beta_{N_1}, \gamma_{N_1}$.

$\overline{N_1'P_1'N_2}$ – $\alpha_{N_2}, \beta_{N_2}, \gamma_{N_2}$.

$\overline{P_1P_1'}$ – $\alpha_P, \beta_P, \gamma_P$.

$\overline{P_1'B}$ – $\alpha_2, \beta_2, \gamma_2$.

$\overline{MB'}$ – $\alpha_M, \beta_M, \gamma_M$.

$\overline{BB'}$ – $\alpha_B, \beta_B, \gamma_B$.

$\overline{O'M}$ – $\alpha_{M'}, \beta_{M'}, \gamma_{M'}$.

Figure 2

degree of the equation, for any particular small section, depends on criteria related to the optical problem. For simplicity here, assume that the coordinates of a number of surface points yield an equation of the form

$$\phi(x,y,z) = a_0 + a_1x + a_2y + a_3x^2 + a_4y^2 + a_5xy - z = 0 . \qquad (2)$$

All of these points can now be taken, one at a time, and the following procedure repeated for each one.

Referring to Figure 2, a point N_1 on the outside surface S_2 is selected. Let the measured coordinates of N_1 in the designer's coordinate system be x_{N_1}, y_{N_1} and z_{N_1}. These coordinates satisfy the equation of the surface.

Therefore,

$$\phi = a_0 + a_1 x_{N_1} + a_2 y_{N_1} + a_3 x_{N_1}^2 + a_4 y_{N_1}^2 + a_5 x_{N_1} y_{N_1} - z_{N_1} = 0. \quad (3)$$

The direction of the principal normal to S_2 at point N_1 is given by

$$\cos \alpha_{N_1} = \frac{\partial \phi / \partial x_{N_1}}{C_{N_1}}, \quad \cos \beta_{N_1} = \frac{\partial \phi / \partial y_{N_1}}{C_{N_1}}$$
$$\text{and} \quad \cos \gamma_{N_1} = \frac{\partial \phi / \partial z_{N_1}}{C_{N_1}} \quad (4)$$

where $\cos \alpha_{N_1}$, $\cos \beta_{N_1}$ and $\cos \gamma_{N_1}$ are the direction cosines of the normal, and C_{N_1} is the square root of the sum of the squares of the partial derivatives of ϕ with respect to x_{N_1}, y_{N_1} and z_{N_1}, or

$$C_{N_1} = \left[\left(\frac{\partial \phi}{\partial x_{N_1}}\right)^2 + \left(\frac{\partial \phi}{\partial y_{N_1}}\right)^2 + \left(\frac{\partial \phi}{\partial z_{N_1}}\right)^2 \right]^{\frac{1}{2}} . \quad (5)$$

The principal normal to S_2 at N_1 meets the inside surface S_1 at a point P_1. The segment $\overline{P_1 N_1}$ is the given thickness t of the windshield and $\overline{P_1 N_1}$ is the principal normal to S_1 at point P_1 because the surfaces are designed parallel.

Let the coordinates of P_1 be x_{P_1}, y_{P_1} and z_{P_1}.

$$\text{By definition,} \quad \cos \alpha_{N_1} = \frac{x_{N_1} - x_{P_1}}{t},$$
$$\cos \beta_{N_1} = \frac{y_{N_1} - y_{P_1}}{t}, \quad (6)$$
$$\text{and,} \quad \cos \gamma_{N_1} = \frac{z_{N_1} - z_{P_1}}{t}.$$

$$\text{So} \quad x_{P_1} = x_{N_1} - t \cos \alpha_{N_1},$$
$$y_{P_1} = y_{N_1} - t \cos \beta_{N_1}, \quad (7)$$
$$\text{and,} \quad z_{P_1} = z_{N_1} - t \cos \gamma_{N_1}.$$

Select a point of observation O′ of given coordinates x_0, y_0 and z_0 in the designer's coordinate system, and let O′ be the origin of a secondary coordinate system whose axes are parallel to the respective designer's axes. $\overrightarrow{O'P_1}$ is the direction of observation.

$$\overline{O'P_1} = d_1 = [\,(x_{P_1} - x_0)^2 + (y_{P_1} - y_0)^2 + (z_{P_1} - z_0)^2\,]^{\frac{1}{2}} \quad , \tag{8}$$

and, by definition,

$$\left.\begin{aligned} \cos\alpha_1 &= \frac{x_{P_1} - x_0}{d_1}, \\ \cos\beta_1 &= \frac{y_{P_1} - y_0}{d_1}, \\ \text{and,}\quad \cos\gamma_1 &= \frac{z_{P_1} - z_0}{d_1}, \end{aligned}\right\} \tag{9}$$

where $\cos\alpha_1$, $\cos\beta_1$ and $\cos\gamma_1$ are the direction cosines of $\overline{O'P_1}$. It is also convenient to express the direction of $\overline{O'P_1}$ by a horizontal angle of scan A and an angle of elevation E.

$$\angle E = \angle(90^\circ - \gamma_1) \, , \tag{10}$$

or

$$\cos E = \sin\gamma_1 \quad . \tag{11}$$

Also $$\cos A \cos E = \cos\alpha_1 \, , \tag{12}$$

therefore, $$\cos A = \frac{\cos\alpha_1}{\sin\gamma_1} \, . \tag{13}$$

The linear segment $\overline{O'P_1}$ defines the direction of observation, but it can also be considered as a light ray which has been transmitted through the windshield after experiencing a refraction at the outside surface and one at the inside surface. To find the direction of the incident ray, it is necessary to determine the path followed by light in the glass and apply the law of refraction at both surfaces. It will be assumed here that the air and the glass are homogeneous media.

The ray of light, in the glass, that intersects surface S_1 at point P_1, and is then refracted in air to point O′, is in the plane of $\overline{P_1O'}$ and the normal $\overline{N_1N_2}$. The angle between this ray and the normal is given by equation (1). Let this incident ray in glass be $\overline{P_1'P_1}$, where point P_1' is the intersection of the ray with surface S_2.

By equation (1),

$$\sin \widehat{P_1' P_1 N_1} = \frac{\mu_{air}}{\mu_{glass}} \sin \widehat{O' P_1 N_2}, \tag{14}$$

angle $O' P_1 N_2$ can be expressed as a function of direction cosines, thus

$$\cos \widehat{O' P_1 N_2} = \cos\alpha_1 \cos\alpha_{N_1} + \cos\beta_1 \cos\beta_{N_1} + \cos\gamma_1 \cos\gamma_{N_1} . \tag{15}$$

Equation (15) gives angle $O' P_1 N_2$ as a function of known parameters, and angle $P_1' P_1 N_1$ can then be calculated from equation (14).

Point P_1' is in the plane determined by points N_1, P_1 and O', and the coordinates of P_1' will satisfy the equation of the plane. Let this equation be

$$A_1 x + B_1 y + C_1 z + 1 = 0 . \tag{16}$$

Substituting the coordinates of each known point, equation (16) gives

$$\left.\begin{aligned} & A_1 x_{N_1} + B_1 y_{N_1} + C_1 z_{N_1} = -1 , \\ & A_1 x_{P_1} + B_1 y_{P_1} + C_1 z_{P_1} = -1 , \\ \text{and,} \quad & A_1 x_0 + B_1 y_0 + C_1 z_0 = -1 . \end{aligned}\right\} \tag{17}$$

Having the three equations (17), the unknowns A_1, B_1 and C_1 can be calculated.

It is now necessary to find the coordinates of point P_1' - x_P, y_P and z_P.

$$\overline{P_1 P_1'} = d_2 = [(x_P - x_{P_1})^2 + (y_P - y_{P_1})^2 + (z_P - z_{P_1})^2]^{\frac{1}{2}} , \tag{18}$$

$$\left.\begin{aligned} \text{and,} \quad \cos\alpha_P &= \frac{x_P - x_{P_1}}{d_2} , \\ \cos\beta_P &= \frac{y_P - y_{P_1}}{d_2} , \\ \cos\gamma_P &= \frac{z_P - z_{P_1}}{d_2} , \end{aligned}\right\} \tag{19}$$

where $\cos\alpha_P$, $\cos\beta_P$ and $\cos\gamma_P$ are the direction cosines of $\overline{P_1 P_1'}$.

The angle between $\overline{P_1' P_1}$ and $\overline{N_1 N_2}$ has been expressed by equation (14), and

$$\cos \widehat{P_1' P_1 N_1} = \cos \alpha_P \cos \alpha_{N_1} + \cos \beta_P \cos \beta_{N_1} + \cos \gamma_P \cos \gamma_{N_1} . \tag{20}$$

Equation (20) can be written

$$d_2 \cdot \cos \widehat{P_1' P_1 N_1} = (x_P - x_{P_1}) \cos \alpha_{N_1} + (y_P - y_{P_1}) \cos \beta_{N_1} + (z_P - z_{P_1}) \cos \gamma_{N_1} , \tag{21}$$

which is a first function of x_P, y_P and z_P.

The coordinates of P_1' satisfy equation (16) because P_1' is in that plane, so

$$A_1 x_P + B_1 y_P + C_1 z_P + 1 = 0 . \tag{22}$$

Equation (22) is a second function of x_P, y_P and z_P.

Point P_1' is also on the outside surface of the windshield, and its coordinates will satisfy the equation of the surface, so

$$\phi = a_0 + a_1 x_P + a_2 y_P + a_3 x_P^2 + a_4 y_P^2 + a_5 x_P y_P - z_P = 0 \tag{23}$$

becomes the third function of x_P, y_P and z_P.

Having three equations (21), (22) and (23), the value of the coordinates x_P, y_P and z_P can be determined.

Note: When the surface equation is of the third, fourth or higher degree, a first approximation for x_P, y_P and z_P is obtained by replacing equation (23) by the equation of the tangent plane to the surface at point N_1. Numerical methods are then used to obtain the exact solution for the coordinates.

The direction of the incident light ray is computed by applying the law of refraction at point P_1' on surface S_2. The direction cosines of the principal normal to S_2 at point P_1' are given by

$$\left.\begin{aligned} \cos \alpha_{N_2} &= \frac{\partial \phi / \partial x_P}{C_P}, \\ \cos \beta_{N_2} &= \frac{\partial \phi / \partial y_P}{C_P}, \\ \text{and,} \quad \cos \gamma_{N_2} &= \frac{\partial \phi / \partial z_P}{C_P}, \end{aligned}\right\} \tag{24}$$

where

$$C_P = [(\frac{\partial \phi}{\partial x_P})^2 + (\frac{\partial \phi}{\partial y_P})^2 + (\frac{\partial \phi}{\partial z_P})^2]^{\frac{1}{2}} , \tag{25}$$

angle $N_1'P_1'P_1$ between the ray $\overline{P_1'P_1}$ and the normal at P_1' is given by

$$\cos \widehat{N_1'P_1'P_1} = \cos \alpha_P \cos \alpha_{N_2} + \cos \beta_P \cos \beta_{N_2} + \cos \gamma_P \cos \gamma_{N_2} , \tag{26}$$

and the angle between the same normal and the incident ray at P_1' is given by

$$\sin \widehat{BP_1'N_2'} = \frac{\mu_{glass}}{\mu_{air}} \cdot \sin \widehat{N_1'P_1'P_1} . \tag{27}$$

Let the coordinates of a point B on the incident ray be x_B, y_B and z_B. The length of the segment $\overline{BP_1'}$ is given by

$$\overline{BP_1'} = d_3 = [(x_B - x_P)^2 + (y_B - y_P)^2 + (z_B - z_P)^2]^{\frac{1}{2}} , \tag{28}$$

and,

$$\left.\begin{aligned} \cos \alpha_2 &= \frac{x_B - x_P}{d_3} , \\ \cos \beta_2 &= \frac{y_B - y_P}{d_3} , \\ \cos \gamma_2 &= \frac{z_B - z_P}{d_3} , \end{aligned}\right\} \tag{29}$$

where $\cos \alpha_2$, $\cos \beta_2$ and $\cos \gamma_2$ are the direction cosines of the incident ray $\overline{BP_1'}$.

The angle of incidence at P_1' is $\widehat{BP_1'N_2'}$ which was obtained in equation (27).

$$\cos \widehat{BP_1'N_2'} = \cos \alpha_2 \cos \alpha_{N_2} + \cos \beta_2 \cos \beta_{N_2} + \cos \gamma_2 \cos \gamma_{N_2} . \tag{30}$$

Replacing the direction cosines by their respective values defined in equation (29),

$$d_3 \cos \widehat{BP_1'N_2'} = (x_B - x_P) \cos \alpha_{N_2} + (y_B - y_P) \cos \beta_{N_2} + (z_B - z_P) \cos \gamma_{N_2} , \tag{31}$$

which is a first function of x_B, y_B and z_B.

The principal normal to surface S_2 at point P_1' meets the inside surface S_1 at point N_1'. Repeating the procedure followed to obtain equation (7), the coordinates of N_1' will be

$$\left.\begin{aligned} x_N &= x_P - t \cos \alpha_{N_2}, \\ y_N &= y_P - t \cos \beta_{N_2}, \\ \text{and,} \quad z_N &= y_P - t \cos \gamma_{N_2}. \end{aligned}\right\} \quad (32)$$

Points P_1', P_1 and N_1' determine a plane which contains the incident ray $\overline{BP_1'}$, and therefore point B.

Again, taking the equation of the plane in the form

$$A_2 x + B_2 y + C_2 z + 1 = 0, \quad (33)$$

and substituting the coordinates of each known point, equation (33) gives

$$\left.\begin{aligned} A_2 x_P + B_2 y_P + C_2 z_P &= -1, \\ A_2 x_{P_1} + B_2 y_{P_1} + C_2 z_{P_1} &= -1, \\ \text{and,} \quad A_2 x_N + B_2 y_N + C_2 z_N &= -1. \end{aligned}\right\} \quad (34)$$

The unknowns A_2, B_2 and C_2 can be determined, and

$$A_2 x_B + B_2 y_B + C_2 z_B + 1 = 0 \quad (35)$$

becomes the second function of x_B, y_B and z_B.

The third function necessary to determine the coordinates of point B will be obtained by selecting an arbitrary vertical plane in the environment where the deviation defined earlier will be measured. For convenience, this plane (P) is chosen perpendicular to the projection, in the horizontal plane, of the observation line and at a distance "d" from O'. Therefore $\overline{O'M} = d$, and the coordinates of point M in plane (P) are

$$\left.\begin{aligned} x_M &= x_0 + d. \cos A, \\ y_M &= y_0 - d. \sin A, \\ \text{and} \quad z_M &= z_0. \end{aligned}\right\} \quad (36)$$

The direction of $\overline{O'M}$ is given by

$$\left.\begin{aligned} \cos \alpha_{M'} &= \cos A, \\ \cos \beta_{M'} &= \cos (90^\circ + A) = - \sin A, \\ \text{and,} \quad \cos \gamma_{M'} &= \cos 90^\circ = 0. \end{aligned}\right\} \quad (37)$$

The general equation of the vertical plane, in terms of its distance from O′ is

$$(x - x_0)\cos\alpha_{M'} + (y - y_0)\cos\beta_{M'} + (z - z_0)\cos\gamma_{M'} - d = 0 . \quad (38)$$

The coordinates of point B will satisfy this equation and,

$$(x_B - x_0)\cos A + (y_B - y_0)(-\sin A) - d = 0 \quad (39)$$

becomes the third function of x_B and y_B.

Equations (31), (35) and (39) yield the values for x_B, y_B and z_B.

The intersection of the observation line with the arbitrary plane (P) at point B′ — $x_{B'}$, $y_{B'}$ and $z_{B'}$ is given by

$$\left.\begin{aligned} x_{B'} &= x_M , \\ y_{B'} &= y_M , \\ \text{and,} \quad z_{B'} &= z_0 + d\ \tan E . \end{aligned}\right\} \quad (40)$$

The deviation, defined as $\overline{BB'}$ is therefore determined since the coordinates of points B and B′ are known.

Two components of the deviation vector are of interest,

$$\left.\begin{aligned} \Delta x &= x_{B'} - x_B , \\ \text{and} \quad \Delta z &= z_{B'} - z_B . \end{aligned}\right\} \quad (41)$$

The component Δy cannot be used because it is a function of the selected arbitrary plane (P). The components Δx and Δz can also be expressed as angles ΔA and ΔE respectively, or combined to give a magnitude and an angle.

CONCLUSION

To obtain a measure of the optical quality of a proposed windshield design, the ray-tracing development is repeated at a sufficient number of surface points for various locations of observation. The integrated effect of deviation vectors over the entire windshield area can be represented, for each observation point, by deviation patterns which can be used for analysis.

The development given in this paper is in its simplest form. More elaborate techniques have been developed to provide for the study of binocular effects.

ACKNOWLEDGMENT

The author wishes to thank Mr. L. Razgunas of the Systems Engineering Department, Engineering Research, Ford Motor Company, for the digital computer programming of the entire analytical development.

4

Fuel Injector Design Problem

By Donald F. Zawoda
Engineering Research and
Advanced Product Study Office
Ford Motor Company

INTRODUCTION

Designing a device which is described by differential equations with variable coefficients which are non-linear, non-analytic functions of one or more variables presents a difficult problem to a design engineer. Although it is often time-consuming and costly to use a design procedure in which successive small changes are made in each and every parameter until the desired result is obtained, when one considers that non-linear equations are not readily solvable and that methods for synthesizing even linear systems are not too well developed, it is not surprising that a trial-and-error method is most often used for designing such a device.

In some cases the number of trial solutions which need be made may be reduced considerably by assuming that the effects produced by one component part of the device can be isolated from the effects caused by the other parts. When an independent causal relationship can be established in this manner, at least one part of the device may be designed comparatively easily and the work of completing the rest of the design may be greatly simplified.

This paper describes how this method of attack was used in designing a fuel injector.

DESCRIPTION OF THE FUEL INJECTOR

The principal parts of the fuel injector are shown in Figure 1. The problem was one of designing the cam and the ports so that fuel would be injected into the cylinder head of an internal combustion engine at a rate which was a predetermined function of the engine speed and time.

At the start of each cycle of operation, the engine-driven cam forces the plunger downward. As ports A, B and C, which connect to the supply port, are closed by the plunger, the pressure of the fuel trapped in chamber C rises. Just as the last of these three

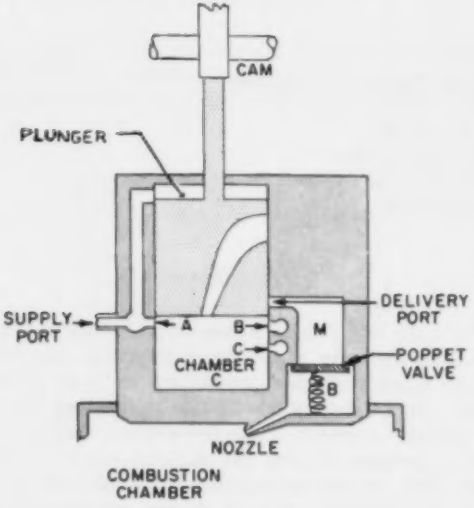

Figure 1. Sketch of the Fuel Injector.

ports closes, the delivery port opens. The resulting surge of fuel from chamber C through the passageway in the plunger and into chamber M causes a rapid buildup of pressure in that chamber. The spring-loaded poppet valve is forced open and fuel flows through the nozzle and into the combustion chamber.

The downward movement of the plunger maintains the nozzle flow at the required rate until port B is opened to chambers C and M through the passageway in the plunger. The pressure in these chambers then falls rapidly, the poppet valve shuts, and flow through the nozzle ceases. Further rotation of the cam returns the plunger to its starting position and the cycle is repeated.

Figure 2 shows the flow rate at which it was desired that fuel be injected through the nozzle. Because a constant quantity of fuel was to be injected during each cycle of operation, the flow rate required was proportional to engine speed and was normalized as shown in the figure. The curve has not been plotted beyond 125° of cam rotation because it was desired only that flow end as quickly as possible at this point. The size of the nozzle and the rate of flow through it were determined from factors relating to the combustion of the fuel which need not concern us here.

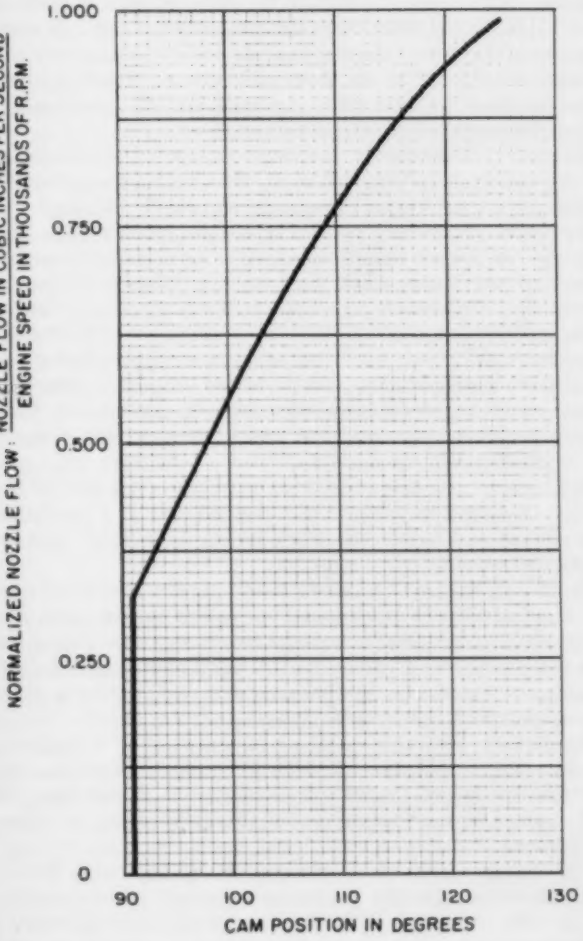

Figure 2. The Desired Flow Rate

DESIGN CONSIDERATIONS

In designing an injector of this type to meet flow rate specifications, two major obstacles are encountered. First, it is possible to

make the injector deliver fuel at the desired rate at only one engine speed. Second, the flow characteristic obtained at any engine speed is determined principally by the size and location of the delivery port and port C, and by the shape of the cam. These system parameters are specified with difficulty because they do not perform their functions independently of one another.

The first difficulty arises because, as the engine speed is increased, the increases in the pressures within the injector are proportionately greater than the change in speed. This causes a larger proportion of the fuel displaced by the plunger to be compressed in chambers B, C, and M. As a result, a smaller volume of the displaced fuel can flow through the nozzle and the flow rate cannot vary linearly with engine speed in the manner desired.

To minimize this effect, the cross sectional area of the plunger, the approximate location of the delivery port, and the total plunger stroke were designed so that the volume of fuel under compression in chamber C would be as small as was practicable at the time the delivery port opened. Likewise, the volumes of chambers B and M were made as small as possible. These quantities were specified at the beginning of the design with no difficulty. The rest of the system was then designed to produce the desired flow at a particular engine speed chosen so that the deviation from the desired flow was within acceptable limits at other speeds.

The difficulty encountered in designing the ports and cam results from the fact that since the delivery port cannot open instantaneously, for all practical purposes, no cam can be devised which will cause the plunger to displace fuel at a rate sufficient to produce the sudden jump in nozzle flow required at 91^{0} of cam position. This jump is approximated by greatly compressing the fuel in chamber C so that there is a sudden surge of fuel through the delivery port as it opens. Thus the flow through the nozzle is a function of the manner in which ports A, B and C close and the delivery port opens, and the shape of the cam after and immediately before the delivery port opens.

The design problem is simplified by assuming that the fuel which flows through the nozzle is obtained from two independent sources: the expansion of the fuel compressed in chamber C before the delivery port opens, and the displacement of fuel by the plunger after the port opens.

Considering only the time after the delivery port opens, for a short interval the fuel compressed in chamber C expands into chamber M. At the same time, of course, most of the fuel displaced by the plunger also flows through the delivery port. After a time the fuel originally compressed in chamber C ceases to expand and a

state of dynamic equilibrium is reached in which the flow through the nozzle becomes dependent solely upon the rate at which the plunger displaces fuel. The time required to reach this equilibrium condition depends to a large degree upon the rate at which the delivery port opens. If this port could open wide instantaneously, the equilibrium would be established virtually instantaneously.

The effect of the initial buildup of the pressure in chamber C, designated hereafter as P_c, diminishes rapidly with time as the delivery port opens. The equations describing the injector can be set up and solved under the assumption that this initial pressure buildup has no effect whatsoever on the nozzle flow. It may be expected that if a cam profile could be found which would yield a solution in which the desired nozzle flow was attained under such a condition, then this cam would also produce the required flow under normal operating conditions if P_c could be made to attain some value which would cause the flow due to the expansion of the fuel compressed in chamber C to make up for the deficiency in flow due to the plunger movement during the time the equilibrium condition was being established.

DESIGN PROCEDURE

Using the procedure outlined above, the profile of the cam was designed from the 91° to the 125° positions by assuming that the desired flow had been established and was being maintained solely by the movement of the plunger.

To accomplish this it was assumed that the cam had rotated through 91°, that ports A, B and C were closed, that the delivery port was fully open, and that the pressures in the various chambers were initially those required to cause the desired flow through the nozzle at the start of the injection portion of the cycle, i.e., at 91° of cam rotation. Under such conditions, the pressure drop across the delivery port would be infinitesimal and chambers C and M could be regarded as one.

Equation 1, the continuity equation, describes the system, but must be modified before being used.

$$(1)\quad A_p \frac{dX}{dt} = \frac{V_{co} - A_p X}{B}\left(\frac{dP_c}{dt}\right) + \frac{V_m}{B}\left(\frac{dP_m}{dt}\right) + \frac{V_b}{B}\left(\frac{dP_b}{dt}\right) + A_n C_q \sqrt{P_n}$$

$$(2)\quad P_c = P_m$$

The symbols are defined as follows:

A_n - Area of nozzle orifice

A_p - Cross sectional area of plunger

B - Bulk modulus of fuel

C_q - Flow coefficient for all ports and orifices

P_b - Pressure in chamber B

P_c - Pressure in chamber C

P_g - Pressure in the combustion chamber (a constant)

P_m - Pressure in chamber M

P_n - Pressure drop across the nozzle

P_s - Supply pressure (a constant)

P_t - Pressure drop across the poppet valve (a constant)

t - Time

V_b - Volume of chamber B

V_{co} - Volume of chamber C with plunger at top dead center

V_m - Volume of chamber M

X - Plunger position measured from top dead center

As can be seen from the equation, it has been assumed that friction in passages and orifices, inertias, head losses, transmission delays, acoustic effects and leakage are all negligible, and that the nozzle is a sharp edged orifice. It can also be assumed that the supply pressure and the combustion chamber pressure are constant.

The poppet valve is designed so that when it is open the pressure drop across it will be virtually constant, regardless of the variation in the flow through it. Since the pressure in chamber M rises rapidly, no great error is introduced by assuming that this valve opens instantaneously when the differential pressure across it equals the constant pressure drop across it when it is open. Thus $P_m - P_b < P_t$ when the valve is closed; $P_m - P_b = P_t$ when it is open.

When the valve is closed, P_b equals P_g. As a result

$$\left.\begin{aligned} P_n &= 0 \quad (3A) \\ \frac{dP_b}{dt} &= 0 \quad (4A) \end{aligned}\right\} \text{ when } P_m < P_g + P_t$$

When the valve is open, P_b equals $P_m - P_t$. Thus

$$\left.\begin{aligned} (3B)\quad & P_n = P_m - P_t - P_g \\ (4B)\quad & \frac{dP_b}{dt} = \frac{dP_m}{dt} \end{aligned}\right\} \quad \text{when } P_m > P_g + P_t$$

If it is assumed that fuel is flowing through the nozzle, the poppet valve must necessarily be open and equations 1, 2, 3B and 4B can be combined to form equation 5.

$$(5)\quad A_p \frac{dX}{dt} = \frac{V_{co} - A_p X + V_m + V_b}{B}\left(\frac{dP_m}{dt}\right) + A_n C_q \sqrt{P_m - P_t - P_g}$$

The last term on the right side of equation 5 is the expression for the rate of flow through the nozzle. This expression was equated to the flow rates desired at a particular engine speed, and P_m was computed and plotted as a function of time. The first derivative of P_m was then used as a forcing function in solving equation 5 for X and its first derivative on an analog computer. Having obtained X in this manner, the shape of the cam profile from 91° to 125° of cam position was known.

Because a portion of the fuel displaced by the plunger remains in compression and never reaches the combustion chamber, as was noted before, a different cam profile was obtained at each engine speed at which equation 5 was solved. Figure 3 shows plunger velocity curves obtained at four different engine speeds. The velocity of the plunger has been normalized by dividing it by the velocity of the cam.

To complete the design a plunger velocity curve was arbitrarily plotted from 125° to 360° of cam position. Since the only important functions the cam performs in this portion of the cycle are to reopen port B as a means of ending flow through the nozzle, and to return the plunger to its starting position, the exact shape of the cam in this region was not critical. Likewise, the velocity curve from 0° to 91° was plotted arbitrarily, care being taken that the plunger would be moved down far enough at 91° so that the volume of fuel in chamber C would be equal to that specified at the beginning of the design. The complete cam profile was then obtained by integrating the plunger velocity function.

From among the family of cam velocity curves which can be plotted, one must be selected which will produce the optimum results over the entire range of speeds at which the engine is to be operated. Ordinarily it is desired that the percentage deviations from the desired flow characteristic be approximately equal in

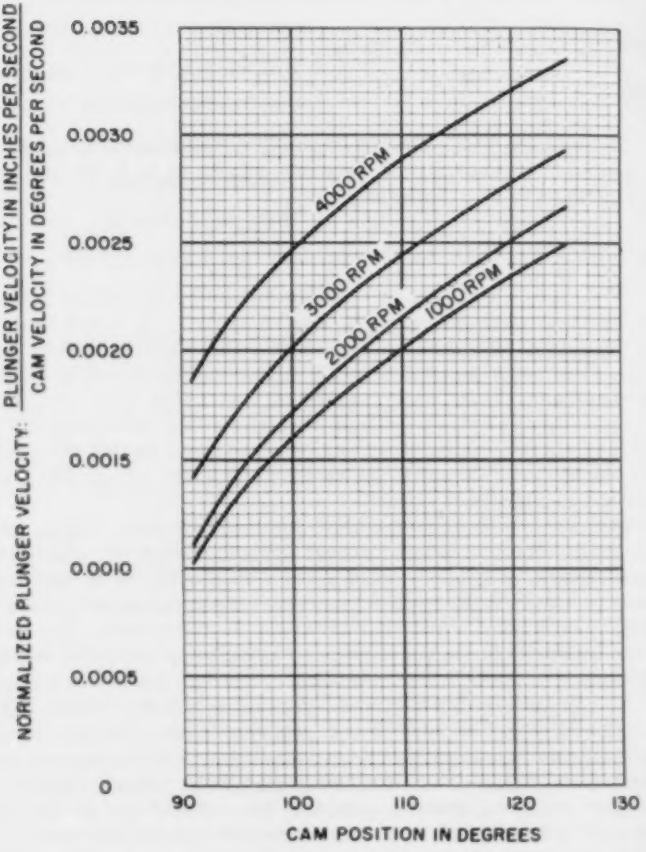

Figure 3. Plunger Velocity Curves Obtained by Solving Equation 5 at Four Engine Speeds.

magnitude at the maximum and minimum engine speeds. Following a rule of thumb, this result can be obtained by solving equation 5 at the engine speed which is the geometric mean of the maximum and minimum speeds. When some other result is desired, several designs of the injector must be completed and evaluated. This was

done in the design described here and the cam obtained at 3000 RPM was judged to perform best.

It was necessary to return to the normal conditions of operation to determine what amount of pressure buildup in P_c would cause the nozzle flow to be the desired value during the time the dynamic equilibrium condition was being established.

The equations for the complete, normal cycle of operation were written by equating the rates of flow into and out of chamber C, and into and out of chambers B and M. The assumptions regarding the poppet valve were used again to simplify the solution.

$$(6)\quad A_p \frac{dX}{dt} = \frac{V_{co} - A_p X}{B}\left(\frac{dP_c}{dt}\right) + A_t C_q \sqrt{P_c - P_s} + A_d C_q \sqrt{P_c - P_m}$$

$$(7A)\quad A_d C_q \sqrt{P_c - P_m} = \frac{V_m}{B}\left(\frac{dP_m}{dt}\right) \text{ when } P_m < P_t + P_g$$

$$(7B)\quad A_d C_q \sqrt{P_c - P_m} = \frac{V_m + V_b}{B}\left(\frac{dP_m}{dt}\right) + A_n C_q \sqrt{P_m - P_t - P_g}$$

$$\text{when } P_m > P_t + P_g$$

The symbols are those used previously, with the following additions:

A_d - Area of delivery port (a function of X)

A_t - Combined area of ports A, B and C, and the effective area of leakage paths in parallel with ports A, B and C (a function of X)

It was assumed that the ports functioned as sharp-edged orifices. Since leakage to the supply port was small and could affect the solution only during the short time all of the ports were simultaneously closed, or almost closed, no great error resulted from representing the leakage paths by a sharp-edged orifice of constant area.

The plunger velocity function obtained at 3000 RPM was used as a forcing function in solving equations 6, 7A and 7B on an analog computer. The pressure buildup required to produce the desired flow rate was most easily determined by trial and error variation of the locations of the ports. This was not a very lengthy process. Ports A and B were designed to close before port C began closing. These two ports and the delivery port were also designed to be fairly large in area; the latter, in order not to impede the flow of fuel at the start of the injection, A and B, in order that chamber C could refull rapidly (through paths not shown in Figure 1) during the return stroke of the plunger. The area of port C was arbitrarily

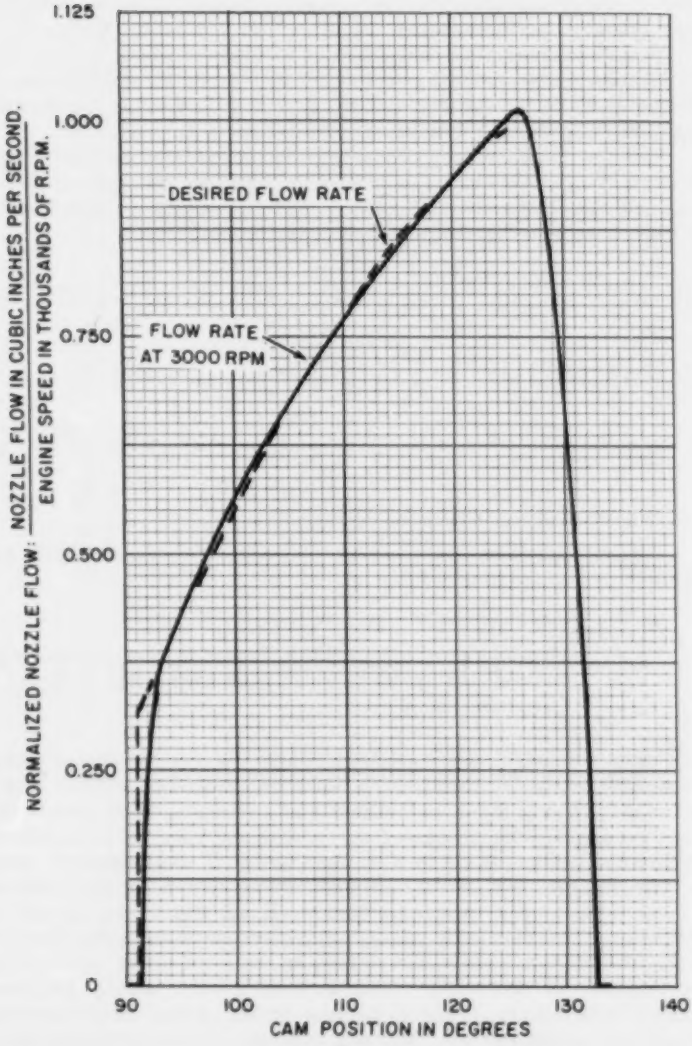

Figure 4. Flow Rate Obtained at 3000 RPM Compared with Desired Flow Rate.

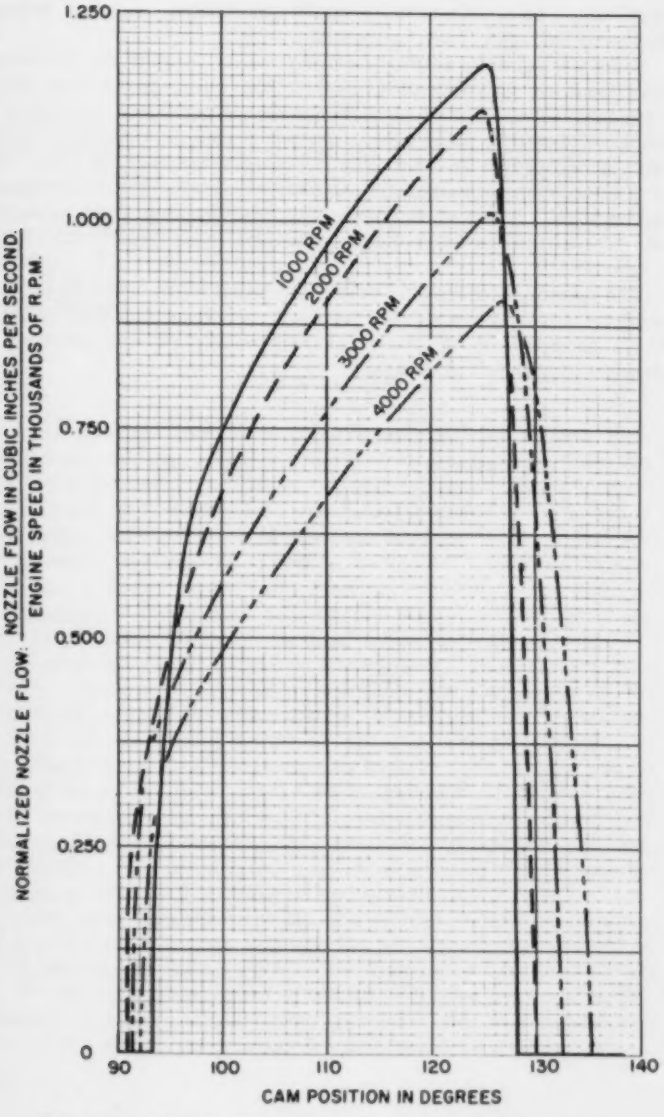

Figure 5. Nozzle Flow Rate at Four Engine Speeds.

specified to be a value which could not produce a large pressure buildup before port C began closing.

Thus the problem merely became one of varying the locations of port C and the delivery port until a flow rate approaching the desired rate was obtained at 3000 RPM. A computer record of the result is shown in Figure 4. Figure 5 shows flow curves obtained from the computer at four different engine speeds. In spite of the many simplifying assumptions which were made in constructing the mathematical model of the injector, data obtained from laboratory tests of an injector correlated quite well with data obtained from the computer.

The assumption, without prior justification, that the effects produced by some parts of the injector could be isolated from the effects produced by the other parts greatly reduced the time required to complete the design.

5

Analysis of Spring Installations for Low-Frequency Suspension of Vehicles

By Raymond R. McHenry
Engineering Staff
Ford Motor Company
Dearborn, Michigan

INTRODUCTION

The primary ride frequencies (bounce and pitch) of modern U.S. automobiles are in the range of 60 to 75 cycles/minute, and the damping level for these oscillations is approximately 25 to 30 percent of critical. Moderate reductions in frequencies (to the range of 40 to 60 cycles/minute) without critical damping can, due to the slower resonant oscillations, produce a ride of a floating nature near the sea-sickness range, in addition to creating serious problems with vehicle height and attitude for static load changes and dynamic weight shift. If load-leveling and some form of compensation for dynamic weight shift are incorporated, the primary ride frequencies should logically be reduced to the range where the damping-force level of the conventional "shock absorber" combination of blow-off valves and hydraulic orifices will provide critical damping (approximately 30 to 40 cycles/minute). A modified form of damping-force diagram has recently been developed for low-frequency suspensions to more readily provide critical damping of ride motions and to eliminate the strike-through problem at the ends of wheel travel (the damping-force is a function of both velocity and *position* of the wheel relative to the vehicle).

In a current-production vehicle the change in wheel load per inch of wheel travel is approximately 10 to 12 percent (referred to sprung portion of wheel load). For a low-frequency vehicle (30 to 40 cycles/minute), the corresponding change must be reduced to approximately 3 percent per inch of wheel travel. For this reason, the geometry of the spring installation is much more critical.

I. CALCULATION OF WHEEL RATES INCLUDING THE EFFECTS OF SPRING INSTALLATION GEOMETRY

Definitions:

L_w = Wheel load (lbs.).

L_s = Spring load (lbs.).

x = Change in spring length from design length (inches, positive in direction which increases spring load).

y = Vertical travel of the tire-to-ground contact point, relative to the vehicle, from design position (inches, positive for movement toward vehicle).

Neglecting dissipative forces, the work done in moving the wheel from its equilibrium position is equal to the potential energy stored in the spring by the corresponding change in spring length. Expressing this in differential form:

$$L_w\,dy = L_s\,dx \tag{1}$$

The rate of change of wheel load with respect to wheel travel (wheel rate) is defined: Wheel Rate = $\frac{dL_w}{dy}$

From equation (1),

$$\frac{dL_w}{dy} = \frac{d}{dy}\left(L_s\frac{dx}{dy}\right) = L_s\frac{d^2x}{dy^2} + \frac{dL_s}{dx}\left(\frac{dx}{dy}\right)^2 \text{ lbs./in.} \tag{2}$$

The spring rate along its own center line, $\frac{dL_s}{dx}$, must be determined from the characteristics of the spring medium.

$x = f(y)$ in some cases can be directly derived from an analysis of the spring-installation geometry (e.g., simple trailing or leading arm suspension). If a functional relationship cannot be derived readily, corresponding values of x and y can be obtained from a digital computer program of the suspension and spring-installation geometry and an empirical polynomial equation can be fitted to this data. In either case, when a functional relationship is obtained between x and y, the first and second derivatives of x with respect to y can be calculated for use in the expression (2) for wheel rate.

The first term of expression (2) is the "geometric rate" due to a non-linear relationship between x and y. A linear relationship $\left(\frac{dx}{dy} = \text{constant}, \frac{d^2x}{dy^2} = 0\right)$ would eliminate the first term and reduce

expression (2) to the generally used approximation for wheel rate (spring rate times nominal installation ratio, $\frac{dx}{dy}$, squared). The first term becomes extremely important for low-frequency suspensions since the required wheel rates produce only a 3 percent change (approximately) in wheel load per inch of wheel travel (e.g., 1000 lb. wheel load, 30 lbs./inch wheel rate). In such an installation, the assumption of a linear relationship between x and y in the calculation of wheel rate for a nominal 0.500 ratio with a rate of change of ratio of ± 1.5 %/inch (± .0075 inch) at design height would produce a ± 50 percent error in the effective design height wheel rate:

From equation (2),

$$\text{the design height wheel rate} = (2000)(\pm .0075) + (120)(.250)$$
$$= 30 \pm 15 \text{ lbs./inch}$$
$$= \text{Nominal} \pm 50\%$$

Since detection of a 1.5 percent change in ratio (dx/dy) per inch of wheel travel is almost impossible by layout drafting methods, low-frequency suspension installations must be analyzed by mathematical methods. The complexity of the functional relationship between x and y will in most cases require a digital computer program to make the analysis practical.

The use of air bags for a spring medium complicates the analysis by introducing a variable load-supporting area. For this reason, the analysis for a gaseous spring medium will be demonstrated with a hydro-pneumatic strut.

II. CALCULATION OF WHEEL RATES FOR HYDRO-PNEUMATIC SPRING MEDIUM

Assumptions:

(1) Ideal gas laws.

(2) Isothermal leveling process.

(3) Polytropic process for dynamic spring action.

(4) Precharge pressure measured with gas at ambient temperature.

Static Gas Volume, $V_1 = \frac{P_0 V_0}{P_1}$ in.^{3} (3)

Where P_0 = Precharge pressure (psia)

P_1 = Pressure under static load (psia)

V_0 = Precharge volume (in.^{3})

From the polytropic process for dynamic spring action:

$$P_2 = P_1 \left(\frac{V_1}{V_2}\right)^k \text{ psia} \tag{4}$$

$V_2 = (V_1 - Ax)$ in.^{3} where x = strut travel from design length (inches, positive in compression).

A = load supporting area (in.^{2})

k = polytropic exponent

$$\therefore P_2 = P_1 \left(\frac{V_1}{V_1 - Ax}\right)^k = \frac{P_1}{\left(1 - \frac{Ax}{V_1}\right)^k} \text{ psia} \tag{5}$$

Strut Load, $$L_S = (P_2 - 14.7)\,A = \frac{P_1 A}{\left(1 - \frac{Ax}{V_1}\right)^k} - 14.7A \text{ lbs.} \tag{6}$$

Strut Rate, $$\frac{dL_S}{dX} = \frac{k\,P_1\,A^2}{V_1\left(1 - \frac{Ax}{V_1}\right)^{k+1}} \text{ lb./in.} \tag{7}$$

By substituting equations (6) and (7) into equation (2) we obtain:

Wheel Rate, $$\frac{dL_W}{dy} = \left[\frac{P_1 A}{\left(1 - \frac{Ax}{V_1}\right)^k} - 14.7\,A\right]\left[\frac{d^2x}{dy^2}\right] + \left[\frac{kP_1A^2}{V_1\left(1 - \frac{Ax}{V_1}\right)^{k+1}}\right]\left[\frac{dx}{dy}\right]^2 \text{ lb./in.} \tag{8}$$

In conventional independent front suspension spring-installations, the $\frac{d^2x}{dy^2}$ term in equations (2) and (8) is negative throughout the range of wheel travel (ratio of $\frac{\text{strut travel}}{\text{wheel travel}}$ larger in extended position than in compressed position). In conventional trailing-arm rear suspensions, the term is positive throughout the range of

travel. The following effects are indicated and have actually been observed on experimental low-frequency vehicles:

(1) As the primary ride frequencies (bounce and pitch) are progressively reduced by decreasing the spring rates, the front suspension becomes unstable.

This instability is due to a non-uniform geometric effect. The "geometric rate" is negative throughout the range of travel; however, it is larger near the extended (rebound) end of travel and it therefore produces a *negative* effective wheel rate in this region of travel when the spring rates are sufficiently reduced.

(2) With gaseous spring media, the variation between static and dynamic spring rates (due to change of the polytropic gas exponent) produces an increased percentage variation in effective front wheel rates and a decreased percentage variation in effective rear wheel rates.

A change in front spring rate appears as a larger percentage change in wheel rate since the effective front wheel rate (equation 8) is the *difference* between the term involving spring rate and the "geometric rate."

The opposite is true on a trailing-arm rear since the effective rear wheel rate is the *sum* of the term involving spring rate and the "geometric rate."

It is readily seen from the described effects that positive values of $\frac{d^2x}{dy^2}$ are desirable from the point of view of exponent changes; however, gas volume requirements dictate that the positive values must be small.

Advantageous application of geometric effects (large negative values of $\frac{d^2x}{dy^2}$ to reduce wheel rates) requires a spring medium with a rate which is insensitive to excitation frequency. For the following, a conventional round wire extension or compression spring will be considered.

III. REDUCTION OF EFFECTIVE WHEEL RATES BY MEANS OF SPRING INSTALLATION GEOMETRY

(1) Geometry required for linear wheel rate from linear spring:

In equation (1), let $L_w = L_{wo} + K_w y$, $L_s = L_{so} + K_s x$ and integrate:

$$\frac{K_s x^2}{2} + L_{so}x = \frac{K_w y^2}{2} + L_{wo}y \qquad (9)$$

Where

K_s = Spring rate (lbs./in.)
K_w = Wheel rate (lbs./in.)
L_{so} = Static spring load (lbs.)
L_{wo} = Static wheel load (lbs.)

The locus of this equation is a hyperbola with center at $\left(-\frac{L_{so}}{K_s}, -\frac{L_{wo}}{K_w}\right)$ or the degenerate case of a pair of intersecting lines if $K_w = K_s\left(\frac{L_{wo}}{L_{so}}\right)^2$.

Solving equation (9) for x and differentiating with respect to y:

$$x = -\frac{L_{so}}{K_s} \pm \sqrt{\left(\frac{K_w}{K_s}\right)y^2 + \left(\frac{2\,L_{wo}}{K_s}\right)y + \left(\frac{L_{so}}{K_s}\right)^2} \qquad (10)$$

$$\frac{dx}{dy} = \frac{L_{wo} + K_w y}{L_{so} + K_s x} \qquad (11)$$

$$\frac{d^2x}{dy^2} = \frac{K_w - K_s\left(\frac{dx}{dy}\right)^2}{L_{so} + K_s x} \qquad (12)$$

(2) Requirements for load-leveling:

If large negative values of $\frac{d^2x}{dy^2}$ are utilized to reduce effective wheel rates, the rates of a system with load-leveling and a fixed relationship between spring and wheel travel will be sensitive to loading. The rate reduction effect will increase with the static spring load (see equation 2), and symmetry of rate-deflection will be altered by load changes.

If critical damping can be obtained for the driver-only condition, the optimum rate vs. static-load relationship would appear to be a compromise between maintaining critical damping (rates decreased as load is increased) and minimizing the effect of friction on height stability. Such a compromise will require determination of the actual form and level of damping as well as measurement of friction. In

order to demonstrate the relationships involved in a system with load-leveling, it will be assumed for simplicity that constant ride frequencies are desired in the following calculations:

$$K_w = L_{wo}\left(\frac{f_d}{187.5}\right)^2 \quad \text{Where } f_d = \text{Design height frequency (cycles/minute)} \tag{13}$$

By substituting equation (13) into equation (12) and letting $x = 0$, we obtain:

$$\left(\frac{d^2x}{dy^2}\right)_o = \left[\frac{dx}{dy}\right]_o\left[\left(\frac{f_d}{187.5}\right)^2 - \left(\frac{K_s}{L_{wo}}\right)\left(\frac{dx}{dy}\right)_o^2\right] \tag{14}$$

The required relationships of the indicated parameters are shown graphically in Figure 1.

Utilization of geometric effects for reduction of effective wheel rates is advantageous from the viewpoints of efficient application of the energy-storing medium and package considerations.

IV. REDUCTION OF REQUIRED VOLUME OF SPRING STEEL BY MEANS OF SPRING INSTALLATION GEOMETRY

Spring Energy at Design Position:

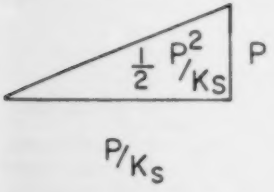

P = Spring load (lbs.)

K_S = Spring rate (lbs./in.)

L_D = Design wheel load (lbs.)

R_D = Design ratio $\left(\frac{\text{spring travel}}{\text{wheel travel}}\right)$

Spring energy $= \frac{1}{2}\frac{P^2}{K_S}$, $P = \frac{L_D}{R_D}$

$$\therefore \text{ Design position spring energy } = \frac{1}{2K_S}\left(\frac{L_D}{R_D}\right)^2 \tag{15}$$

Δ Energy in Spring = Δ Energy at Wheel:

By means of ratio variation effects, the effective wheel rate produced by a linear spring can assume a variety of forms. For this study, two forms of wheel rate will be considered:

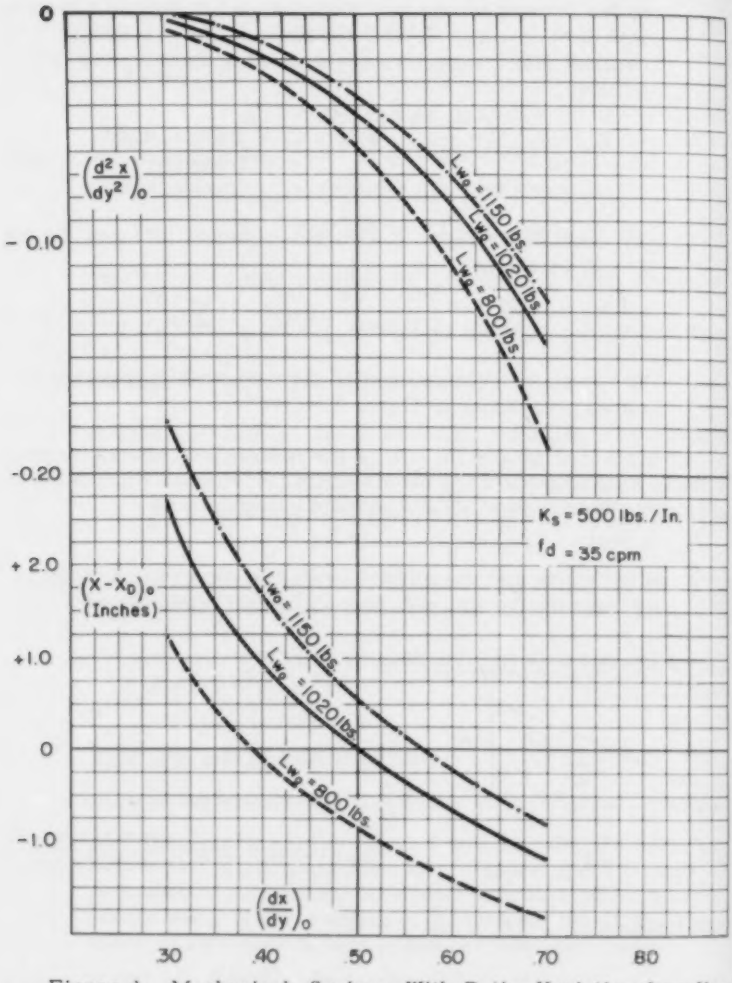

Figure 1. Mechanical Springs With Ratio Variation-Leveling Requirements For Constant Frequency System.

(1) $K_w = K_{wo}$ = Constant (produced by a hyperbolic relationship between spring and wheel displacement including the degenerate case of a hyperbola which is a straight line).

(2) $K_w = K_{wo} + K_{w1} y^2$ = Symmetrical rate build-up (parabolic rate curve).

The two cases will be covered by solving for case (2) and letting $K_{w1} = 0$ to produce case (1).

$K_w = K_{wo} + K_{w1} y^2$, for 4.5 inch maximum wheel travel:

$K_{wm} = K_{wo} + 20.25\ K_{w1}$

$$\frac{K_{wm}}{K_{wo}} = 1 + 20.25\left(\frac{K_{w1}}{K_{wo}}\right), \text{ let } \frac{K_{wm}/K_{wo}-1}{20.25} = \alpha,\ K_{w1} = \alpha K_{wo}$$

$$K_w = K_{wo}(1 + \alpha y^2) \tag{16}$$

$$\text{Wheel load} = L_D + K_{wo}\int_0^y (1 + \alpha y^2)\,dy = L_D + K_{wo}\left(y + \frac{\alpha}{3} y^3\right) \tag{17}$$

$$\Delta \text{ Energy} = \int_0^y \left(L_D + K_{wo} y + \frac{K_{wo}\alpha}{3} y^3\right) dy = L_D y + \frac{K_{wo}}{2} y^2 + \frac{K_{wo}\alpha y^4}{12} \tag{18}$$

$$\underline{\text{Maximum Spring Energy}} = \frac{1}{2K_s}\left(\frac{L_D}{R_D}\right)^2 + L_D y + \frac{K_{wo} y^2}{2} + \frac{K_{wo}\alpha y^4}{12} \tag{19}$$

let $\beta = \dfrac{K_{wo}}{K_s (R_D)^2}$, $\delta = \dfrac{L_D}{K_{wo}}$

$$E_{max} = \frac{L_D}{2}\left(\beta\delta + 2y + \frac{y^2}{\delta} + \frac{\alpha y^4}{6\delta}\right) \tag{20}$$

let $y_{max} = 4.5$ inches

$$\text{Maximum Spring Energy, } E_{max} = \frac{L_D}{2}\left(\beta\delta + 9 + \frac{20.25}{\delta} + 68.344\frac{\alpha}{\delta}\right)$$

$$\delta = \frac{L_D}{K_{wo}} = \left(\frac{187.5}{f_D}\right)^2$$

$$E_{max} = \frac{L_D}{2}\left[9 + \beta\left(\frac{187.5}{f_D}\right)^2 + (5.76 \times 10^{-4})(f_D^2)(1 + 3.38\,\alpha)\right] \tag{21}$$

Active Volume Required in Round Wire Compression and Extension Springs:

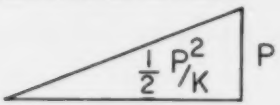

$$E = \frac{1}{2}\frac{P^2}{K}$$

$$f = P/K$$

$$\left.\begin{aligned} K &= \frac{P}{f} = \frac{Gd^4}{8ND^3} \\ P &= \frac{\pi Sd^3}{8D} \end{aligned}\right\} \quad E = \frac{1}{2}\frac{P^2}{K} = \left(\frac{1}{2}\right)\left(\frac{\pi^2 S^2 d^6}{64 D^2}\right)\left(\frac{8ND^3}{Gd^4}\right) = \frac{\pi^2 S^2 d^2 ND}{16G} \qquad (22)$$

$$\text{Active Volume} = (N)(\pi D)\left(\frac{\pi d^2}{4}\right) = \frac{\pi^2 d^2 ND}{4}$$

$$\therefore \text{ Energy} = \frac{S^2 V}{4G} \text{ inch-lbs., } V (\text{in.}^3) = \left(\frac{4G}{S^2}\right) E \qquad (23)$$

$$\text{Active Volume Required} = \frac{2G\, L_D}{S^2}\left[9 + \beta\left(\frac{187.5}{f_D}\right)^2 + (5.76 \times 10^{-4})(f_D^2)(1 + 3.38\,\alpha)\right]$$

Let $G = 11.5 \times 10^6$, $L_D = 1{,}100$ lbs., S (uncorrected) = 110,000 psi

$$V = 2.09\left[9 + \beta\left(\frac{187.5}{f_D}\right)^2 + (5.76 \times 10^{-4})(f_D^2)(1 + 3.38\,\alpha)\right] \text{in.}^3 \qquad (24)$$

Where f_D = Design height frequency (cpm)

$$\beta = \frac{K_{wo}}{K_s (R_D)^2}$$

$$\alpha = \frac{K_{wm}/K_{wo}^{-1}}{20.25}$$

Figure 2 shows the effect of variation of β on active spring steel volume requirements for the following two cases:

(1) Constant wheel rate ($\alpha = 0$).

(2) Parabolic wheel rate with rate at full travel double that at design height ($\alpha = 0.0494$).

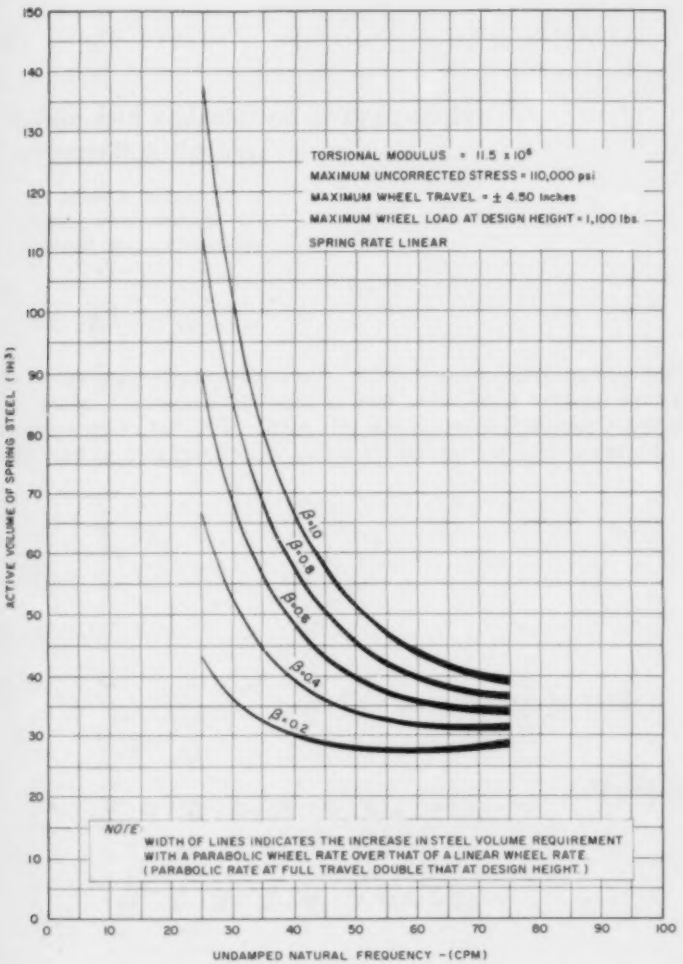

Figure 2. Required Active Volume of Spring Steel vs. Frequency. (Round wire compression and extension springs.)

6

Design and Calculation of Progressive Compression Springs

By Albert E. Roller
Pontiac Motor Division
General Motors Corporation

1. INTRODUCTION

This analysis deals with round wire helical compression springs in which a progressive rate is produced by means of a varying number of active coils. With the derivation of a simple equation by integration it is possible to calculate the rate of such a spring.

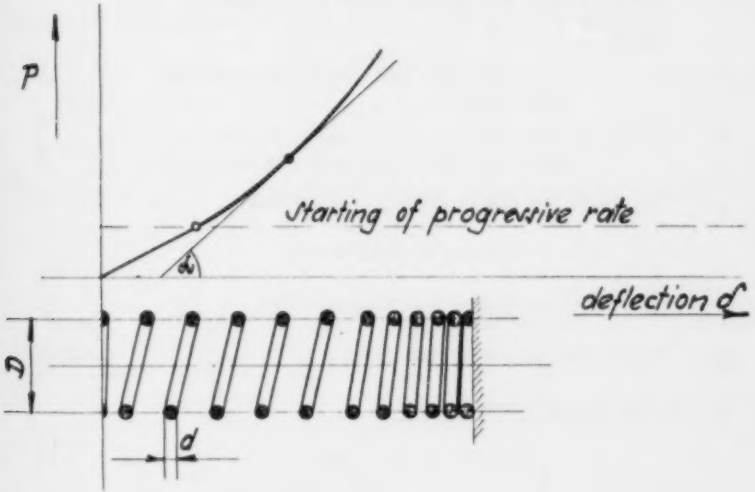

Figure 1

In most ordinary springs, deflection is directly proportional to load. Sometimes, however, progressive rate is a requirement. It is possible to design a compression spring with a definitely increasing rate (e.g. by using a variable pitch of coils). During deflection of

such a spring, touching of coils starts at any point depending on the spring design. This reduces the number of active coils and increases the rate of the spring. A spring working under these conditions may be called a progressive spring.

Symbols.

G	= Torsional modulus of rigidity	$lb.in^{-2}$
d	= Diameter of wire	inch.
D	= Mean diameter of coils	inch.
n	= Full number of active coils before touching of coils	
n_p	= Number of eliminated coils at deflection δ_p	
n_a	= Number of active coils depending on deflection	
c	= Rate of spring	$lb.in^{-1}$
δ	= Deflection of spring	inch.
δ_p	= Deflection of spring between progressive limits	inch.
P	= Load on spring	lbs.
S_s	= Shear stress	$lb.in^{-2}$
k	= Stress factor for spring design depending on ratio $\frac{D}{d}$	
τ	= $k \times S_s$ = Resultant shearing stress when stress-factor applied	$lb.in^{-2}$
f	= $\frac{30}{\pi}\sqrt{\frac{c}{m}}$ = Frequency in cycles per min when applied load on spring is $P = m \times g$	
g	= Acceleration due to gravity = (12)(32.2)	$inch.sec^{-2}$
a	= $\frac{8\ D^3}{d^4 G}\ n$ = Factor for simplification	
b	= $\frac{8\ D^3}{d^4 G} \times \frac{n_p}{\delta_p}$ = Factor for simplification	
W	= Work done on the spring	inch.lbs.

Feature of progressive springs.

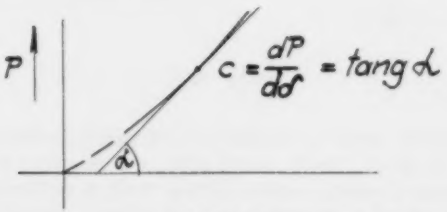

Figure 2

If the frequency $f = \frac{60}{2\pi} \cdot \omega = \frac{30}{\pi}\sqrt{\frac{c}{m}}$ is to be constant in the range of the progressive spring rate, the ratio $\frac{c}{m}$ must be constant.

From this results the derivation,

$$\omega^2 = \frac{c}{m} = \frac{dP}{d\delta} \cdot \frac{g}{P}$$

$$\delta = \frac{g}{\omega^2} \int \frac{dP}{P} = \frac{g}{\omega^2} \ln \frac{P}{P_0}$$

$$\boxed{P = P_0 \times e^{\frac{\delta\omega^2}{g}}} \qquad (1)$$

Equation (1) indicates that the spring rate follows the law of the exponential function

$$y = e^{ax}$$

In this function all curves intersect the ordinate y at unit 1,

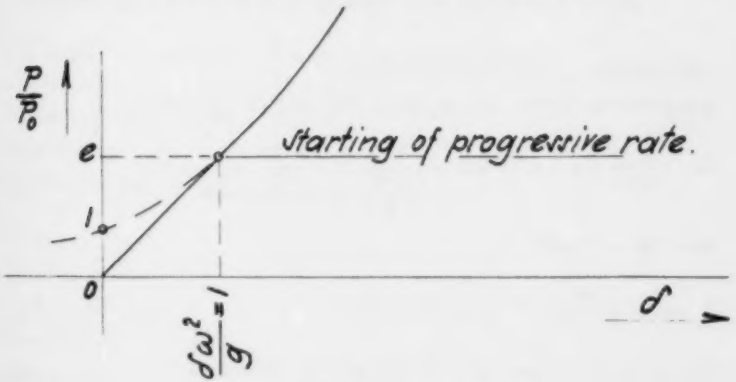

Figure 3 (for $\frac{c}{m}$ = const. only)

2. General Relations for a Progressive Compressive Round Wire Helical Spring.

From the known relation for this type of spring,

$$d\delta = \frac{8 D^3}{d^4 G} \cdot n_a \cdot dP \qquad (2)$$

it will be recognized that a deviation of $\frac{dP}{d\delta}$, the rate of spring, is only possible by changing the number of active coils. This can be arranged by producing a spring with variable pitch of coils operating as explained in the introduction. The following analysis provides a method of computing progressive springs.

If the design of a spring provides for the elimination of active coils in proportion to deflection δ, the number of eliminated coils will be,

$$\delta \cdot \frac{n_p}{\delta_p} \qquad \text{(See Fig. 4)}$$

Therefore the number of active coils as a function of deflection,

$$n_a = n - \delta \frac{n_p}{\delta_p} \qquad (2a)$$

Point A in fig. 4 where coils begin to roll off may be determined according to the requirements of the spring application.

Note, Considering fig. 4 the spring calculation has to be made in parts. For range O-A the ordinary spring equations are applied. For range A-B the following equations can be used.

Development of the Basic Equation.

Substituting the value of n_a from (2a) into (2) we obtain,

$$d\delta = \frac{8\,D^3}{d^4G}\left[n - \delta \frac{n_p}{\delta_p}\right]dP = \left[\underbrace{\frac{8\,D^3}{d^4G}\,n}_{a} - \underbrace{\frac{8\,D^3}{d^4G} \cdot \frac{n_p}{\delta_p}}_{b}\,\delta\right]dP$$

$$d\delta = (a - b\delta)dP$$

$$P = \int \frac{d\delta}{a - b\delta} = -\frac{1}{b} \ln (a - b\delta) + C$$

For point A we get, $P = O$ and $\delta = O$ therefore

$$O = -\frac{1}{b} \ln a + C$$

$$C = \frac{1}{b} \ln a$$

$$P = \frac{1}{b}\left[\ln a - \ln (a - b\delta)\right] = \frac{1}{b} \ln \frac{1}{1 - \frac{b}{a}\delta}$$

$$P = \frac{1}{b} [\ln 1 - \ln (1 - \frac{b}{a} \delta)]$$

$$\boxed{P = - \frac{1}{b} \ln (1 - \frac{b}{a} \delta)} \qquad (3)$$

This is the basic equation for progressive spring rate between point A and B in fig. 4 where,

$$\frac{b}{a} = \frac{n_p}{n \cdot \delta_p} \quad \text{and} \quad b = \frac{8\ D^3}{d^4 G} \cdot \frac{n_p}{\delta_p}$$

Conversion of the basic equation shows that it is possible to solve mathematically,

$$e^{-bP} = 1 - \frac{b}{a} \delta$$

$$\boxed{\delta = \frac{a}{b} [1 - e^{-bP}]} \qquad (3a)$$

For $n = n_p$ it will be $\frac{b}{a} = \frac{1}{\delta_p}$

For $\delta = \delta_p$ it will be $\frac{b}{a} \times \delta = \frac{n_p}{n}$ and we find

$$\boxed{P = - \frac{1}{b} \ln (1 - \frac{n_p}{n})} \qquad (3b)$$

From (3b) we get,

$$e^{-bP} = 1 - \frac{n_p}{n}$$

$$\boxed{n = \frac{n_p}{1 - e^{-bP}}} \qquad (3c)$$

Furthermore,

$$- bP \times \log e = \log(1 - \frac{n_p}{n})$$

$$- \frac{8\ D^3}{d^4 G} \cdot \frac{n_p}{\delta_p} \cdot P \cdot \log e = \log(1 - \frac{n_p}{n})$$

$$\boxed{\delta_p = - \frac{8\ D^3}{d^4 G} \cdot n_p \cdot P \cdot \frac{\log e}{\log(1 - \frac{n_p}{n})}} \qquad \log e = 0.43429 \qquad (4)$$

Note, For elimination of active coils in proportion to deflection δ, any other function can be used. In the case that a solution by integration is impossible a graphic method usually will be satisfactory.

3. Stress Formula.

Computing of stresses, of course, will be the same as in ordinary compressive springs.

Therefore shearing stress at inside of coil,

$$\tau = \frac{8\,D}{\pi\,d^3} \cdot P \cdot k \qquad \text{lb.in}^{-2} \qquad (5)$$

k = "Wahl correction factor"

Note, Within the progressive range do not calculate the stresses in proportion to deflection as often is done when computing ordinary springs. In this case the stresses must be calculated by using the force P because P is not proportional to deflection.

4. Work done on the spring.

Considering fig. 4 again, we see that the work must be computed by parts.

For the range O-A (triangle OAD) we get,

$$W_1 = \frac{P_A \cdot \delta}{2} \qquad \text{inch.lb.} \qquad \text{where } P_A = \text{Force at point A.}$$

For the range A-B,

Area ABC,

$$W_2 = \int_{\delta=0}^{\delta=\delta_p} P\,d\delta = \int_0^{\delta_p} -\frac{1}{b} \ln\left(1 - \frac{b}{a}\delta\right) d\delta$$

$$= -\frac{1}{b} \int_0^{\delta_p} \ln\left(1 - \frac{b}{a}\delta\right) d\delta$$

For $1 - \frac{b}{a}\delta = V$ we get

$$W_2 = \frac{a}{b^2} \int_0^{\delta_p} \ln V \cdot dV = \frac{a}{b^2} [V \cdot \ln V - V]_0^{\delta_p}$$

$$= \frac{a}{b^2} \{ [1 - \frac{b}{a} \delta] \ln (1 - \frac{b}{a} \delta) - [1 - \frac{b}{a} \delta] \}_0^{\delta_p}$$

and within the limits,

$$\boxed{W_2 = \frac{a}{b} \cdot \frac{1}{b} \{ [1 - \frac{b}{a} \delta_p] [\ln (1 - \frac{b}{a} \delta_p) - 1] + 1 \}} \qquad (6)$$

Area ACED,

$W_3 = P_A \cdot \delta_p$

Total work done on spring therefore,

$W = W_1 + W_2 + W_3$ inch.lb.

Example, Design of a helical progressive compression spring with the following assumed data,

Wire diameter	$d = 5/16''$
Mean diameter of coils	$D_m = 2''$
Number of active coils at point B	$n_a = n_B = 4{,}5$
Maximum load on spring at point B	$P_B = 500$ lbs.
Load on spring at point A	$P_A = 200$ lbs.
Spring index $\frac{D_m}{d} = 6{,}4$	
Stress factor $k = 1.23$	
Torsional modulus of rigidity for steel	$G = 11.5 \times 10^6$ lb.in^{-2}

Solution, (See also Fig. 4)

Maximum shearing stress at inside of coil,

$$\tau_{max} = \frac{8 D}{\pi d^3} \cdot P_B \cdot k = \frac{8 \cdot 2}{\pi \times 0.3125^3} \times 500 \times 1.23 = \underline{102\,600} \text{ lb.in}^{-2}$$

Spring rate at point B,

$$C_B = \frac{dP}{d\delta} = \frac{d^4 \cdot G}{8 \cdot D^3 \cdot n_B} = \frac{0.3125^4 \times 11.5 \times 10^6}{8 \times 2^3 \times 4.5} = \underline{381} \text{ lb.in}^{-1}$$

Frequency

$$f = \frac{30}{\pi} \cdot \sqrt{\frac{c}{m}} = \frac{30}{\pi} \sqrt{\frac{381 \times 12 \times 32.2}{500}} = \underline{164} \text{ min}^{-1}$$

If equal frequency at point A and B is desired we obtain the spring rate at range O-A,

$$C_0 = C_B \frac{P_A}{P_B} = 381 \frac{200}{500} = \underline{152.5} \quad \text{lb.in.}^{-1}$$

Full number of active coils before touching of coils,

$$n = \frac{d^4 G}{8 D^3 C_0} = n_B \frac{C_B}{C_0} = 4.5 \frac{381}{152.5} = \underline{11.25} \text{ coils}$$

Therefore the number of eliminated coils at deflection δ_p from point A to point B,

$$n_p = n - n_a = 11.25 - 4.5 = \underline{6.75} \text{ coils}$$

Deflection from O to A,

$$\delta = \frac{P_A}{C_0} = \frac{200}{152.5} = \underline{1.31} \text{ in.}$$

Deflection from A to B by using equation (4)

$$\delta_p = -\frac{8 D^3}{d^4 G} n_p (P_B - P_A) \frac{\log e}{\log(1 - \frac{n_p}{n})}$$

$$\delta_p = -\frac{8 \times 2^3}{0.3125^4 \times 11.5 \times 10^6} \times 6.75 \times (500 - 200) \frac{0.43\,429}{0.60206 - 1} = \underline{1.29} \text{ in.}$$

$$b = \frac{8 D^3}{d^4 G} \cdot \frac{n_p}{\delta_p} = \frac{8 \times 2^3}{0.3125^4 \times 11.5 \times 10^6} \cdot \frac{6.75}{1.29} = \frac{1}{327}$$

$$\frac{b}{a} = \frac{n_p}{n \cdot \delta_p} = \frac{6.75}{11.25 \times 1.29} = \frac{1}{2.15}$$

Calculation of curve A-B,

δ inch.	$\frac{b}{a}\delta$	$1 - \frac{b}{a}\delta$	$\ln(1 - \frac{b}{a}\delta)$	$P = -\frac{1}{b}\ln(1 - \frac{b}{a}\delta)$
0	0	1	0	0 lbs.
0.2	0.093	0.907	6.81014 - 6.90776 = - 0.0976	32 lbs.
0.4	0.186	0.814	6.70196 - 6.90776 = - 0.2058	67 lbs.
0.6	0.279	0.721	6.58064 - 6.90776 = - 0.3271	107 lbs.
0.8	0.372	0.628	6.44254 - 6.90776 = - 0.4652	152 lbs.
1.0	0.465	0.535	6.28227 - 6.90776 = - 0.6255	205 lbs.
1.2	0.558	0.442	6.09131 - 6.90776 = - 0.8165	267 lbs.
1.29	0.600	0.400	5.99146 - 6.90776 = - 0.9163	300 lbs.

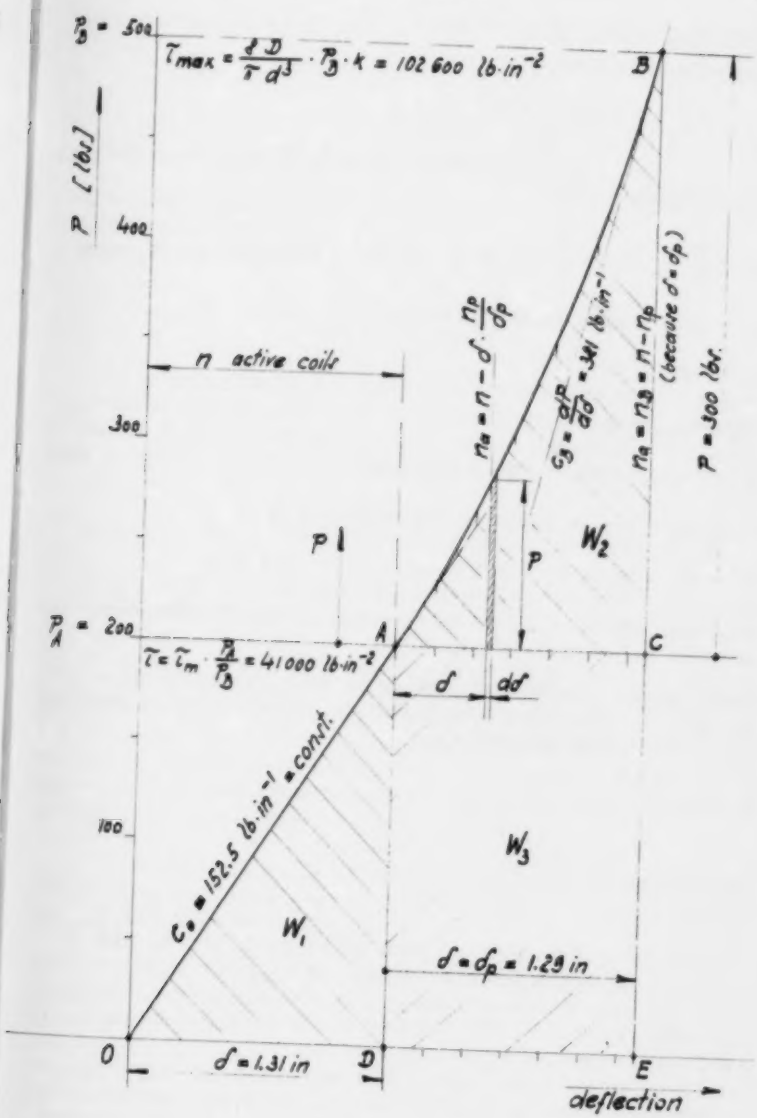
P_B = 500
τ_max = (d/r d³) · P_B · k = 102 600 lb·in⁻²
B
P [lbs]
400
n active coils
300
n_a = n − δ · n_p/δ_p
c_3 = δ_p/δ = 341 lb·in⁻¹
n_a = n_B = n − n_p
(because δ = δ_p)
P = 300 lbs.
P
W_2
P_A = 200
A
C
τ = τ_m · P_A/P_B = 41000 lb·in⁻²
δ
dδ
c_0 = 152.5 lb·in⁻¹ = const.
100
W_3
W_1
δ = δ_p = 1.29 in
0
δ = 1.31 in
D
E
deflection

Figure 4

Work done on the spring see fig. 4,

Regarding area OAD,

$$W_1 = \frac{P_A \cdot \delta}{2} = \frac{200 \times 1.31}{2} = 131 \text{ in.lb.}$$

Regarding area ABC,

$$W_2 = \frac{a}{b} \cdot \frac{1}{b} \left\{ \left[1 - \frac{b}{a} \delta_p \right] \left[\ln \left(1 - \frac{b}{a} \delta_p \right) - 1 \right] + 1 \right\}$$

$$W_2 = 2.15 \times 327 \left\{ [0.400] [- 0.9163 - 1] + 1 \right\}$$

$$W_2 = 165 \text{ in.lb.}$$

Regarding area ACED,

$$W_3 = P_A \delta_p = 200 \cdot 1.29 = 258 \text{ in.lb.}$$

Total work done on spring during deflection O-B,

$$W = W_1 + W_2 + W_3 = 131 + 165 + 258 = \underline{554} \text{ in.lb.}$$

This example is based on the assumption that the frequency for points A and B is the same.

Based on the equation outlined above most requirements in progressive compression spring design can be calculated as practised in common spring computation.

7

Experiences with Highly Loaded Gearing

By Forest McFarland
Buick Division
General Motors Corporation

INTRODUCTION

As a result of seeing its application for many years, I am very conscious of the importance of mathematics to engineering design. I hope in this discussion to relate some experiences in actual designs and developments which may be of value to you.

GEARING IN LAY SHAFT AUTOMOBILE TRANSMISSIONS

In the early thirties, attention began to be paid to making the gearing in automobile transmissions not only durable but quiet. To do this, engineers began to employ helical gearing. It was not enough simply to cut, harden, and assemble the gears – several rules had to be followed. I will describe the requirements for satisfactory operation, found as a result of the development of the first Packard helical gear transmission, in which I had a part, under the direction of W. R. Griswold, then Chief Research Engineer. A later version of this transmission employing the same principle of gearing is shown in Figure 1.

1. The gears must be cut and "shaved" very accurately for lead, profile, and index. These particular gears were also lapped by the "Incolap" method.
2. The profile of the gears must be accurately held, but primarily must be designed to provide "soft" contact at the start of engagement, which means modifying the involute. Figure 2 shows a typical profile deviation chart. You will note from the modification charts the action is from the pitch point on, or recess action. I have been told that the old clocks with wooden teeth employed mainly recess action. I have not seen it, but have mentally theorized on benefits of this action and suspect a good case can be made for it with gearing of questionable efficiency.

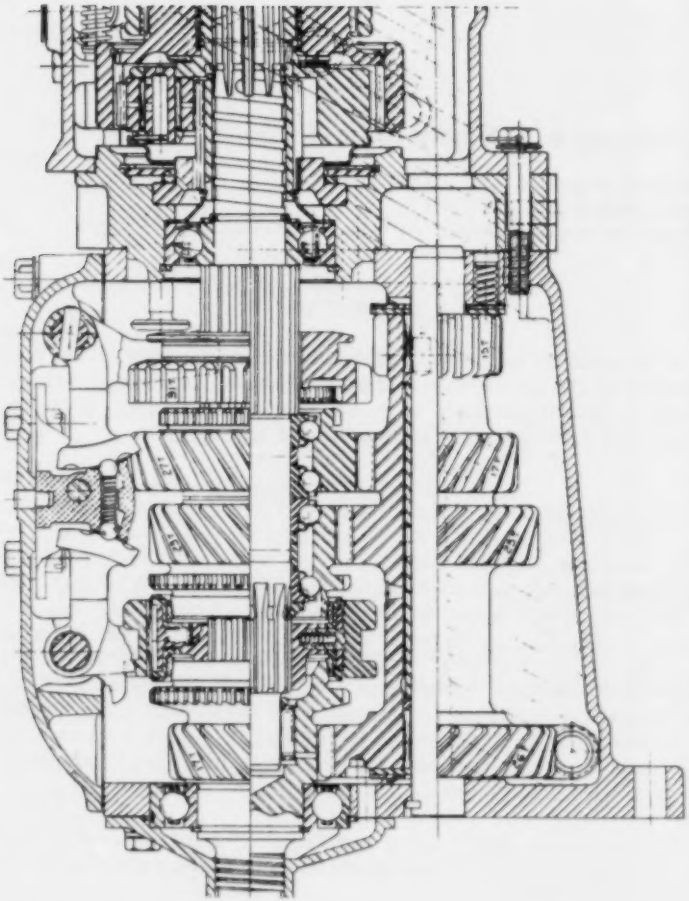

Figure 1. Packard Helical Gear Transmission

Figure 1. Packard Helical Gear Transmission

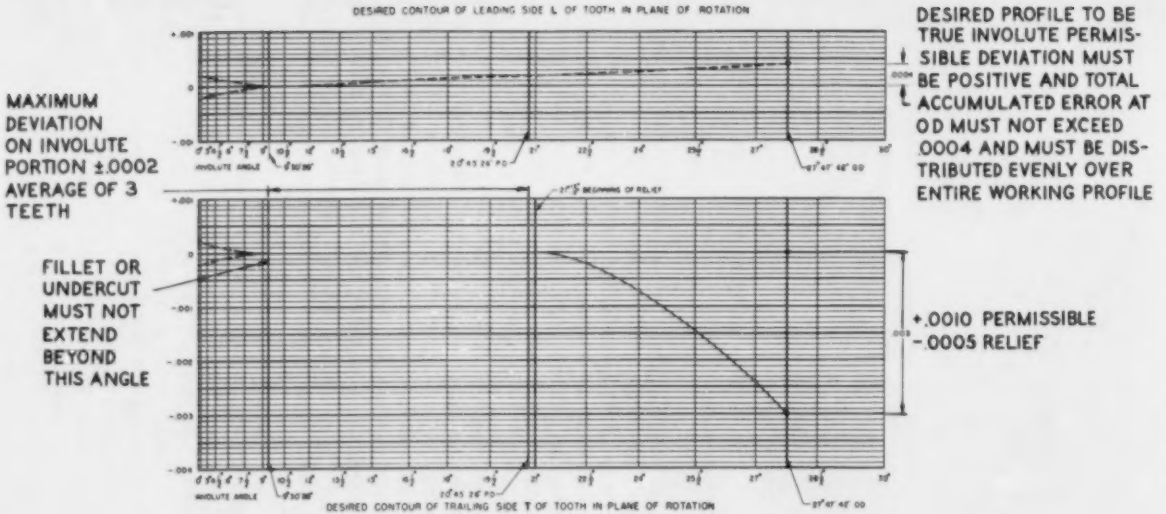
DESIRED CONTOUR OF LEADING SIDE L OF TOOTH IN PLANE OF ROTATION
MAXIMUM DEVIATION ON INVOLUTE PORTION ±.0002 AVERAGE OF 3 TEETH
DESIRED PROFILE TO BE TRUE INVOLUTE PERMISSIBLE DEVIATION MUST BE POSITIVE AND TOTAL ACCUMULATED ERROR AT OD MUST NOT EXCEED .0004 AND MUST BE DISTRIBUTED EVENLY OVER ENTIRE WORKING PROFILE
FILLET OR UNDERCUT MUST NOT EXTEND BEYOND THIS ANGLE
+.0010 PERMISSIBLE
-.0005 RELIEF
DESIRED CONTOUR OF TRAILING SIDE T OF TOOTH IN PLANE OF ROTATION

Figure 2. Typical Profile Deviation Chart

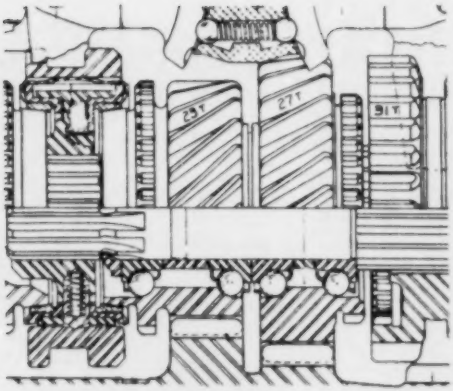

Figure 3. Rigid Ball Bearing Gear Mounting.

3. The gears should have a helical contact ratio of two or more if possible. Helical contact ratio appears "worth more" than involute contact ratio to reduce deflection and reduce "PV" values. Angles on the constant mesh gears of over 45^0 were called for in the forward constant mesh gears and angles of the same lead, of course, in the first and second speed gears, to balance the countershaft end thrust.

4. The gears must be rigidly and accurately mounted. High helix angles make this problem more difficult. Figure 3 shows ball bearing mountings in two of the gears. This was a development all in itself. The completed transmission is again shown in Figure 1. This unit was extremely quiet and very rugged. It was practically impossible to determine whether the car was in second gear or direct drive except by engine speed. High helix angles make for more expensive mountings, but the additional cost was felt to be justified in this case.

Since transmission gears operate at full engine torque only a small percent of their life, the question arose as to what stresses could be allowed. The most realistic work I know of was done by J. O. Almen and John Straub, published in the middle Thirties, when they were with General Motors Research. Their method, briefly, was to examine the service life of various transmissions, calculate the stresses by a modified Lewis formula and then run these units at full torque in first and second gear. The results showed that a transmission good for 100,000 cycles in first gear and 300,000 in second would give satisfactory life in service.

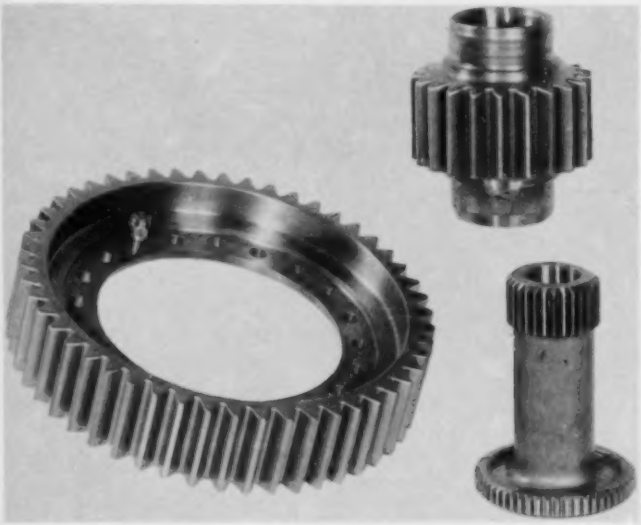

Figure 4. Rolls-Royce Aircraft Gears

REAR AXLE GEARING

Hypoid rear axle gearing, introduced by Packard in 1924, has become standard in the industry. In the design of rear axle gearing, we are again "plagued" by deflections which cause the contact to move particularly lengthwise on the gear teeth. As is true of many other parts, rear axle gear-set components are designed primarily for stiffness rather than for strength. The gears cut by the Gleason process provide deflection of the parts by a "crowning" effect of the teeth to keep the contact "on the teeth" rather than over the edge of the teeth. This applies particularly lengthwise on the teeth but also to the tip of the teeth. The more the deflection, the more must be the "crowning." It is, therefore, highly important that the mountings be kept very rigid to keep deflection to a minimum; to minimize crowning; to keep Hertz stresses to a minimum; to insure capacity and also to keep spiral overlap to a maximum for quietness. Deflection tests are run on the gearing in drive and coast, and the results very carefully studied. Balance, of course, must be obtained in the design. It is desirable that the contact under no load be in the vicinity of the middle of the teeth and stay there under load. As a result of a careful analysis on the writer's part of the effect of each individual deflection on movement of the bearing along the gear face

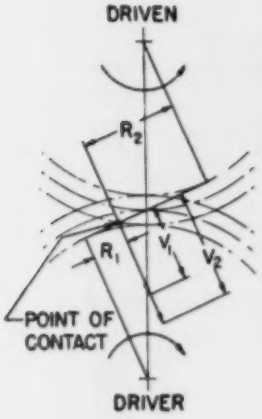

SLIDING OCCURS PERPENDICULAR TO LINE OF ACTION AT THE POINT OF CONTACT. THE VELOCITY VECTORS V_1 AND V_2 HAVE INSTANTANEOUS TANGENTIAL VELOCITIES AROUND THEIR RESPECTIVE CENTERS OF ROTATION AS INDICATED BELOW

$$\frac{\text{R.P.M.(DRIVER)}}{60} \times \frac{2\pi}{12} \times R_1 = V_1 \frac{FT}{SEC}$$

$$\frac{\text{R.P.M.(DRIVEN)}}{60} \times \frac{2\pi}{12} \times R_2 = V_2 \text{ "}$$

$$\text{SLIDING VELOCITY} = (V_2 - V_1) \text{ "}$$

$$\text{SURFACE STRESS} = \sqrt{\frac{0.35 \times \text{NOR. FORCE}\left(\frac{1}{R_1} + \frac{1}{R_2}\right)}{\text{FACE WIDTH}\left(\frac{1}{E_1} + \frac{1}{E_2}\right)}} = P$$

$$P.V. = P \times (V_2 - V_1) = \frac{\#}{IN.^2} \cdot \frac{FT}{SEC.}$$

Figure 5. Surface Stress & PV Values

of the particular gear set studied, it was concluded that stiffening the pinion shank, particularly at the rearward end, provided more control of contact for the money expended than any other one item of design. As a result, the largest rear bearing bore commercially feasible was worked into this design. This was provided even to the extent of obtaining a cone of special inside diameter. The results finally obtained from this design were gratifying, as the gear set was definitely smaller than several others, even though behind the largest engine in the industry at that time.

AIRCRAFT ENGINE GEARS

During the last war, the writer had the opportunity to observe the behavior of the gears (approximately eighty in number) of the Rolls-Royce Merlin Engine as produced by Packard. The most challenging problem was the elimination of "scuffing" — a combination of pitting and scoring in the reduction gears which were very highly loaded, being approximately 4,000 lb.-per-inch of face at the start of production and ending up at approximately 6,300 lb.-per-inch of face on the final "dash 9" production engines, operating in an engine oil with no particular anti-scuff additives.

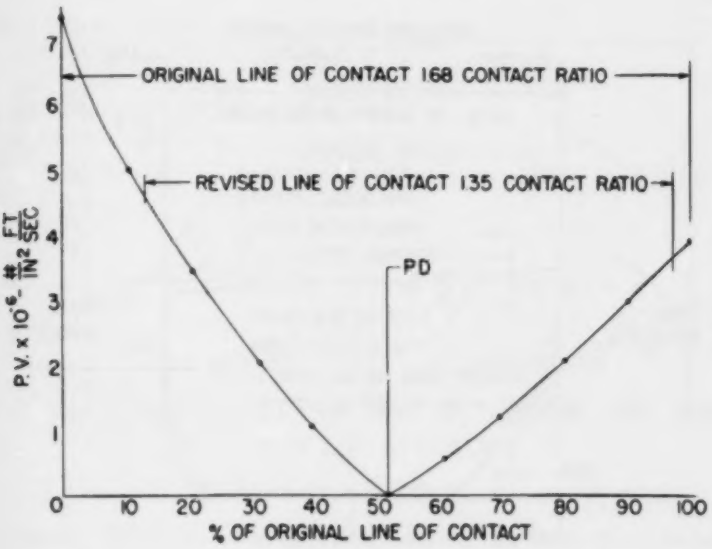

Figure 6. PV Values for One Set of Teeth in Action

A tremendous amount of work was done on this gear-set. It was found that trouble-free operation required:-

1. Proper profile of teeth.
2. Accurate mounting of gears in good alignment.
3. Parallelism of teeth within close limits.
4. Proper surface finish on teeth.
5. Adequate lubrication at right times.

Solution of this problem was very elusive as we could repeatedly prove that violation of any one of these items would not cause trouble if the other items were within proper limits. This was a case where pure "logic" would lead one astray. Taking sufficient liberties with any two or three items gave trouble. I am mentioning this point in particular as I have seen the same situation arise in other troubles resulting in long, drawn-out arguments between Manufacturing and Engineering. The only answer I know is for Management and Manufacturing to have confidence in Engineering, but at the same time people in Engineering must do enough work to be sure they are right.

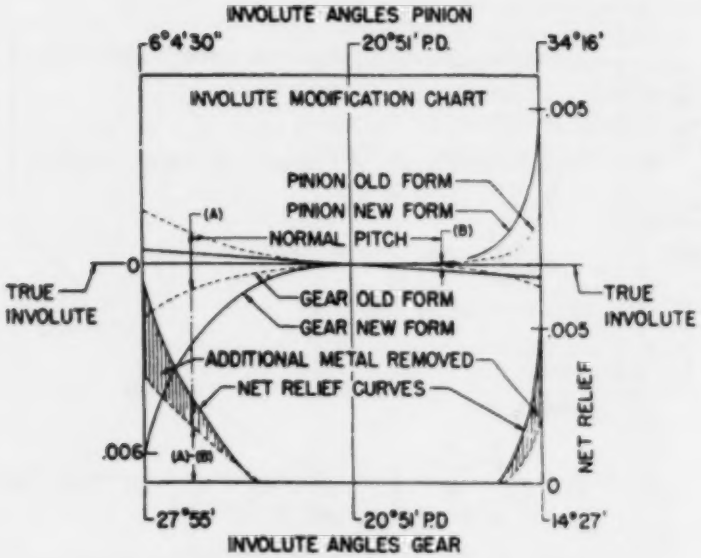

Figure 7. Pinion & Gear Tooth Modification

Since this investigation was so fruitful and can be applied to other situations, it is believed worthwhile to discuss the items just mentioned in detail.

PROFILE

A layout was made of the gears shown in Figure 4. The surface pressure was determined by the Hertz method, and the sliding velocity of the gear tooth surfaces calculated. The product of these two values was taken for each point of contact, under the assumption that only one mesh of teeth carries the load through the action, as the proper division of load between two sets of teeth in mesh is difficult to obtain. The method of calculation is shown in Figure 5. It is somewhat similar to that used by Almen in calculating PV values of rear-axle gears. Since the product of the pressure and a frictional coefficient and sliding velocity should represent a measure of the power loss or heat dissipation for each instant of time, it was felt the action should be balanced so this product of pressure and sliding velocity is the same at each end of the action. The

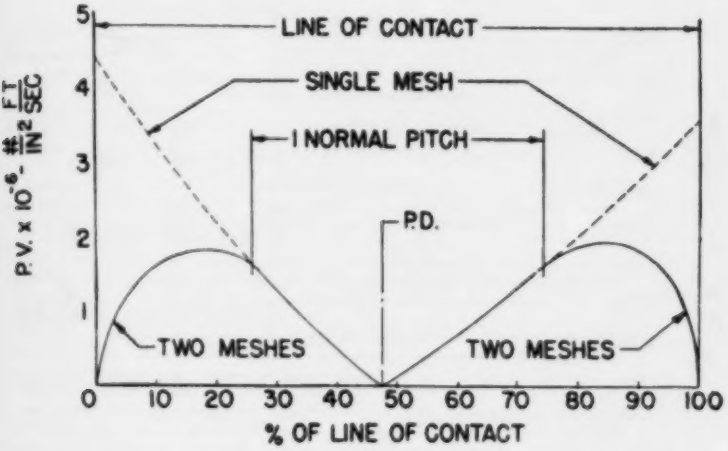
LINE OF CONTACT
SINGLE MESH
1 NORMAL PITCH
P.D.
TWO MESHES
TWO MESHES
P.V. x 10⁻⁶ - #/IN² FT/SEC
% OF LINE OF CONTACT
0 10 20 30 40 50 60 70 80 90 100
1 2 3 4 5

Figure 8. PV Values for Two Sets of Teeth in Action

frictional coefficient was assumed constant for each given value of pressure. The products of pressure and sliding velocity were designated PV values to agree with previously-established nomenclature. The actual PV value is admittedly zero at each end of the action, but by balancing the values at the start and end of action, the ends of the single-mesh action will also be substantially balanced.

Figure 6 shows the PV values for one set of teeth in action. The original and revised length of action is indicated. The original contact ratio of 1.68 reduces to 1.35. This indicates that contact ratio by itself is not a good measure of gear capacity. These figures and the test experience resulted in increasing the amount of metal removed from the form of the gear and the pinion teeth, as shown in Figure 7. This figure shows the pinion tooth modification above the zero line and the gear tooth modification below it. The action of the teeth moves from left to right. Clearance A (between respective contacting points at the root of the pinion and tip of the gear at the start of action) minus clearance B (between the contacting points of the teeth in the preceding mesh) represents the net clearance or "net relief" which is shown in the lower part of the chart. This relief prevents undue contact pressure which would result from the deflection of the teeth in the preceding mesh under load. The increase in the clearance or net relief is shown by the shaded area in the net relief chart. The changes shown in Figure 7 balanced the action of the gears so that scuffing tendencies should occur no more at the start of action than at the end.

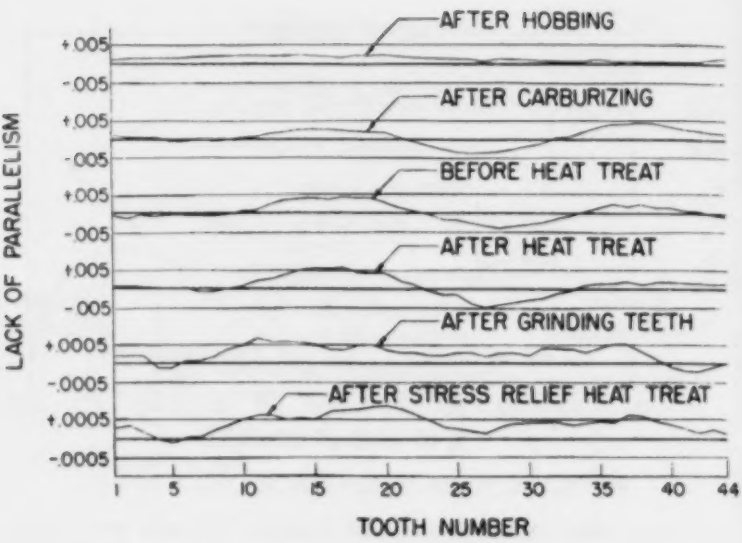

Figure 9. Parallelism of Gear Teeth

Figure 8 shows an estimated curve of actual PV values considering two sets of teeth in contact compared to the "single mesh" values for one set.

MOUNTING

The method given by Rolls-Royce for aligning the gears at the time Packard started production consisted of bluing the teeth in assembly to secure a heavy bearing at the rear of the teeth, by swinging the reduction gear cover in a rabbet concentric with the propeller shaft, and then doweling the cover in place.

A careful check on approximately 200 engines indicated that scuffing appeared more frequently at the rear of the teeth when the bearing was heavy at the rear. Deflection tests of the gears in a four-square type of test fixture were carefully analyzed. They indicated that the axes of the gears assumed a new position equivalent to being transposed parallel to their original axes. This information resulted in doweling the reduction gear cover to the crankcase with the pinion bearing bores in line and parallel to the reduction gear bearing bores. Better bearing across the teeth was obtained from this procedure.

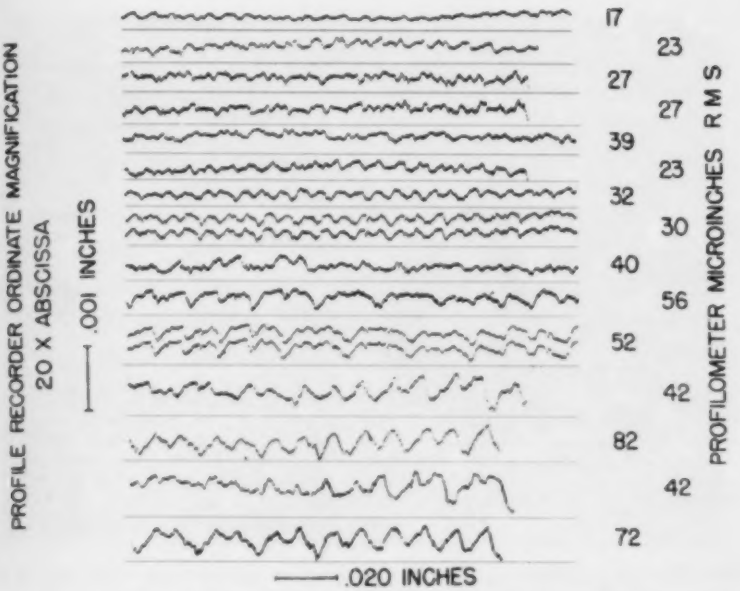

Figure 10. Surface Roughness Measurement

PARALLELISM

When the gears were blued-in, a considerable variation in parallelism of the teeth was observed, clusters of five or six teeth being out of line. Very careful parallelism checks of every tooth in each of a dozen reduction gears were made after each step of the processing. A record of the checks on one gear is shown in Figure 9.

It was found that most of the distortion occurred in carburizing, the gears going out-of-flat as well as out-of-round. A change in processing eliminated this trouble. It was also found that when the gears were too much out-of-parallel before grinding, it was difficult to remove all the error by grinding. The teeth of the reduction gear and the pinion were finally held parallel within 0.0003″ in the width of the tooth without difficulty. Parallelism has been stressed, as it has been found much more difficult to maintain than proper index. Since little difficulty was experienced in maintaining index within 0.0002″ between the adjacent teeth of these gears, the effect of index errors on scuffing was not determined.

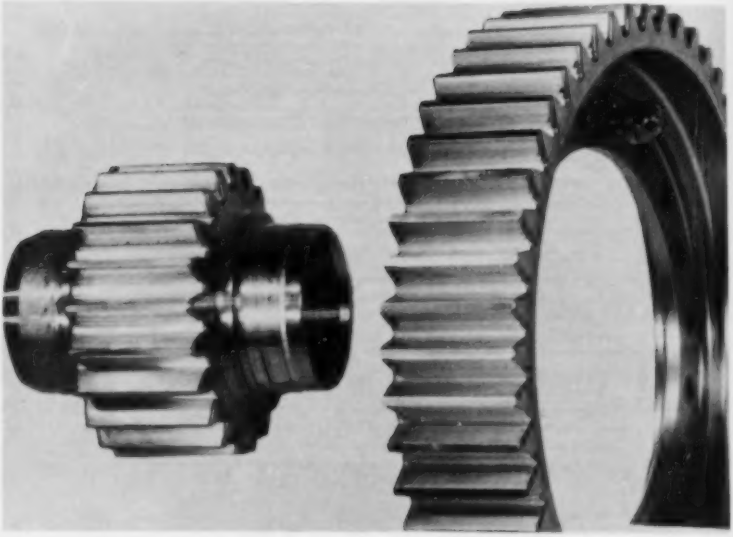

Figure 11. Reduction Gears After Model Test

SURFACE FINISH

In order to improve the grinding technique, the grinding wheels were dressed coarser with the dressing diamonds. Wheels dressed too fine tended to load up, particularly at one point, and give a pattern which appeared to be the result of a vertical bounce and horizontal oscillation, apparently induced by the exciting force of the loaded wheel. This pattern consisted of alternate high and low spots on the teeth, those on one side of the tooth space being displaced from those on the opposite side by the distance the table traveled during one-half wheel revolution. Coarser dressing eliminated this difficulty and also reduced magnaflux checks, particularly at the roots of the teeth.

Observation of a large number of the gears after the acceptance run indicated the coarser finish showed less marking and "fussiness" than the fine finish. Comparison of the profilometer readings with profile recorder charts, as shown in Figure 10, led to specifying surfaces to be made in accordance with samples to obtain the character of surface found desirable. Finishes, in agreement with the samples, were accepted between profilometer readings of 15 to 37 root mean square. Under proper conditions, gears of this type of

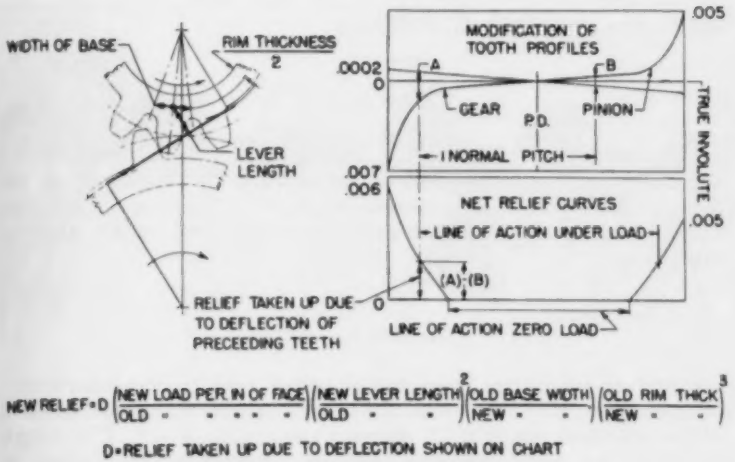

Figure 12. Empirical Formula for Comparing Tooth Deflection of Comparable Gear Structure

finish will go through a model test without wearing through the grinding marks. Figure 11 shows a set of gears after model-test.

As a result of the improvement in gear tooth finish, the same method of finishing was applied to camshaft rocker levers. Revision of the finish specification from 10 maximum profilometer reading to new limits of 15 to 23 resulted in a distinct improvement after acceptance runs.

This finish was applied to steel gears running with steel gears only. In one instance it was found necessary to make a crossed axis helical steel gear smoother to prevent it from cutting the mating bronze gear.

LUBRICATION

Improper lubrication at the start of the acceptance runs was suspected. A pump was installed on one dynamometer stand which was started when priming the engine, and was run until 10 minutes after starting under power. The record of scuffed gears of this stand for approximately 175 engines was compared to the general average of all the other stands, and a very definite improvement was noted. The acceptance test schedule was revised to call for priming lubrication of the reduction gears before starting the

engine, and continuing until 10 minutes after firing, to ensure sufficient oil to run in the gears properly.

SUMMARY

Careful attention to all the details listed resulted in reducing scuffing, from an objectionable percentage of rejections in the factory, to less than 0.5%. Service experience has shown that if the gears do not scuff during the acceptance run, they are not likely to scuff in service.

NEW GEAR DESIGN

Further anticipated increases in power indicated the desirability of more capacity in the reduction gears. A new design was studied with a pressure angle of 25 degrees and a pitch of 4.1. The length of action decided upon was based on permitting PV values of 3,000,000 at each end, resulting in a contact ratio of 1.25. After establishing the usable action, the gear teeth were proportioned for strength. The modification was then established, using the previous deflection data of the production gears and applying the empirical formula shown in Figure 12.

It will be noted that the teeth are assumed as deflecting about a point in the middle of the rim. Calculation of the deflection of a tooth as a non-uniform beam will account for only a small percentage of the actual deflection present. The tooth actually bends as a body under load. The net relief shown below the modification chart equals A minus B as noted on the chart for start of action. A is taken where contact actually starts, and the net relief represents the clearance necessary to provide for the deflection of the teeth under load in the preceding mesh.

Between the point of first contact and the outside radius of the gear, there is a ramp of 0.030″ length on the gear tooth. Visual inspection of this ramp indicates if the contact is starting where desired. This determines if the proper amount of net relief has been provided. This also enables one to establish the amount of deflection in the preceding teeth by referring to the charts of the gears observed. The net relief at the end of action is established using the same procedure.

The ramp at the tip is very important to assure that first contact does not extend to the tip of the gear tooth. The radii of curvature of both gear teeth should contact without loss of area to keep the unit pressure down and improve lubrication.

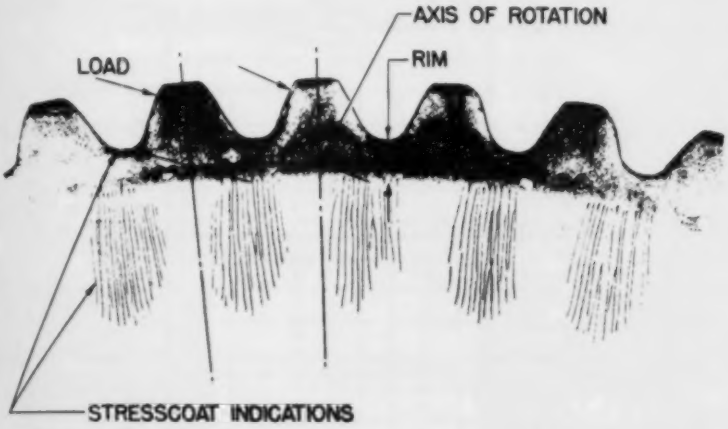

Figure 13. Reduction Gear Stresscoat Study

The stresscoat checks, as shown in Figure 13, help to confirm the theory that the gear tooth deflects about a point in the center of the rim.

Figure 14 shows the final modification charts for the gear and pinion as they appear on the respective engineering drawings. They have been matched together to enable the net relief to be determined. Separate charts were kept as a permanent record of each set of production gears.

A closed circuit reduction gear fixture, shown diagrammatically in Figure 15, was designed and built to test the new gears at loads in excess of engine loads. Loading of the gears was accomplished by winding up a calibrated torsion shaft between the reduction gear pinions by the turnbuckles on one propeller shaft flange. The torsion shaft was enclosed and supported in a tube to provide lateral stiffness. On this fixture the test gears were lubricated and cooled by low-pressure jets of oil directed into the mesh, as in the engine. The dummy gears at the opposite end were lubricated by high-pressure oil jets on the teeth after mesh. The dummy gears were first lubricated by an e-p oil of SAE 90 viscosity to give them more surface capacity than the test gears. Later, engine oil was used, but in greater quantities than on the test gears.

Test running of the new gears indicated their capacity to be appreciably greater than that of the original gears. The action started and ended where called for by the design, with no scuffing except when overloaded appreciably, with the result that no change

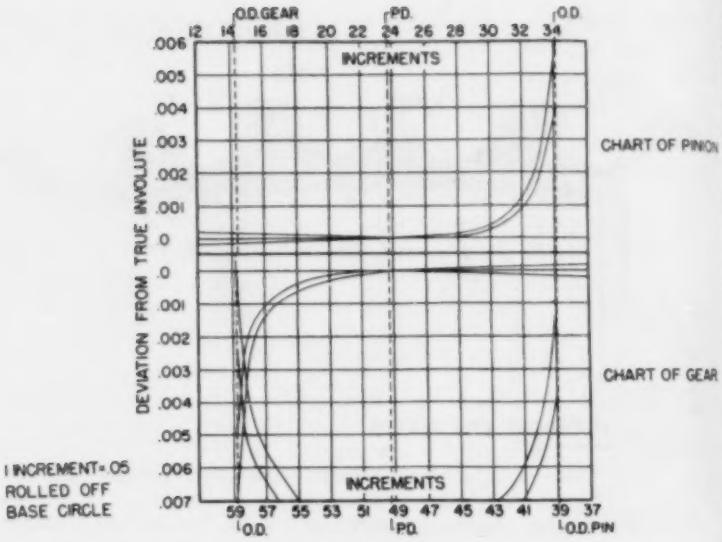

Figure 14. Modification Charts

whatever was made in the modification established in the original design. A year and a half of production experience with no scuffing indicated no change necessary. The modification formula has been used on several other gear-sets and found satisfactory, but is offered with hesitance since a large number of different gear designs have not been checked. Care must be used in obtaining the original deflection data. The designs compared should have the same general structure.

The closed circuit test fixture gave an opportunity to determine the efficiency of the gears, which was approximately 99% per mesh.

PLANETARY GEARING

Planetary gearing, used in overdrives in the thirties, has come into prominence in automatic transmissions, particularly since World War II. These gear sets will carry large powers for their sizes because the load is divided between several meshes of gears. Alignment of the teeth is very favorable, with regard to deflections of mountings, and the product of the loads and the pitch line velocities (or more properly the base circle velocities) is ordinarily

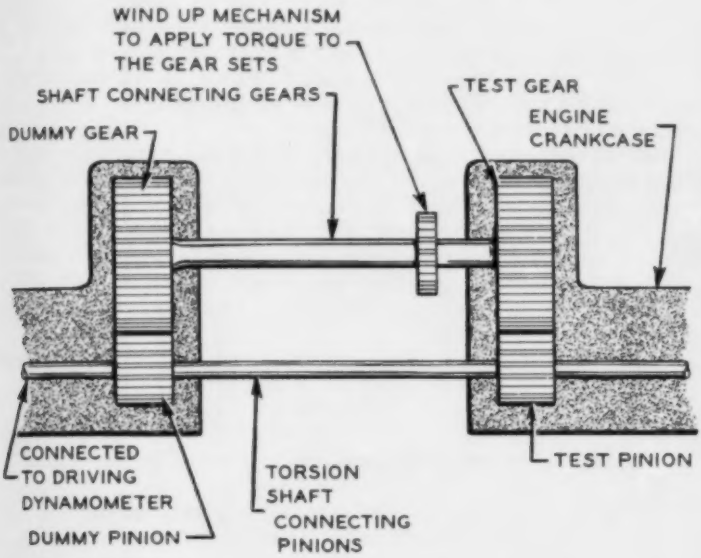

Figure 15. Diagram of Reduction Gear Test Fixture

not as large for a given reduction as in multiple reduction layshaft gearing in series. Strictly speaking, the power loss in the gearing would not be measured directly by base radius velocities-times-load-times-a factor, but the load on the teeth-times-a "suitable" coefficient-times-the sliding velocity on the teeth summed up over the line of action. Determination of load on the teeth where two sets are in mesh is, of course, not easy.

Reduction of power loss is as important in keeping the teeth cool to avoid distress as to save fuel. Proper lubrication of teeth is extremely important. This applied also to needle bearings, particularly those supporting the pinions. I recall one case in which the gear-set, with marginal lubrication as furnished in the production unit, permitted the pinion needle bearings to weld in approximately 30 minutes under full engine torque. Adequate lubrication to the bearings enabled the gears to run 50 hours without distress except pitting of the pins on which the needle bearings ran. This pitting started rather early, but we continued to run the gear-set without any ill effects until considerable pitting had occurred; but with the set still entirely operable. That raises the question as to when we should classify a unit as "failed" due to pitting.

Modification of the involute is desirable on planetary gearing, but from the writer's experience, appears to be only enough to prevent interference on start of action; as the deflections appear to be less than those on gear trains like aircraft reduction gears as described. In any case, one can look at the teeth and see where contact starts. That is the final answer.

Helical contact ratios of the order of 1.3 to 1.4 have resulted in satisfactory quietness in gear sets with which the writer is familiar. These ratios can be obtained due to the finer teeth, with helix angles of the order of 18 to 20 degrees, without excessive gear width. This makes axial thrust and gear tooth lead alignment problems easier. Very slight crowing of teeth and very slight cutting of pinion teeth "off lead" has been attempted at times to maintain proper bearing on the teeth.

CONCLUSION

To make highly-loaded gearing work successfully, we should:

1. Make mountings as stiff and as accurate as possible to secure accurate alignment of tooth faces. If there is flexibility, it should be of a nature that causes the teeth to align and not misalign themselves.
2. Make gearing accurate for lead or parallelism. To be successful, gearing must be held more accurately than the production people are willing to see shown on the drawings.
3. Modify the teeth properly to suit the conditions to which they are subject. An analysis will show you can run on only about so much of the profile due to excessive sliding if you go too far under high loading.
4. Secure proper surface finish to suit the conditions present.
5. Provide proper lubrication, particularly at start of operation.
6. Secure the best balance between surface durability and beam strength of the teeth in the original design. We make teeth fine to obtain surface durability; we make them coarse to obtain beam strength. Breakage of teeth is, of course, a greater hazard than scuffing or scoring them, but gearing has been over-designed in this regard at the expense of surface durability.
7. PV values as described in this paper or PVT values as developed by Almen and Straub are the best methods the writer knows for determining surface capacity of gear teeth. PVT values were developed to overcome one defect of PV values which showed up under large variation of pitch line speeds and sliding. We used PV values because of our experience background.

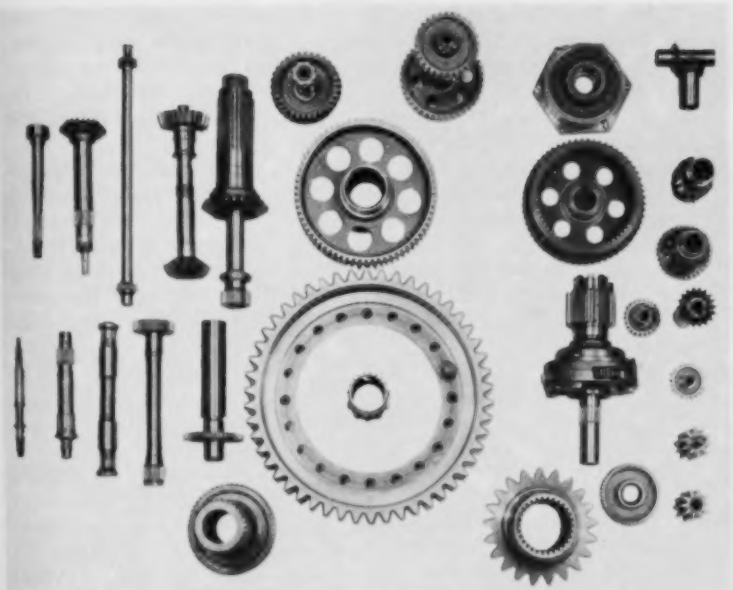

Figure 16. Major Gears-Rolls-Royce Aircraft Engine

By observing the rules just listed, we were able to make all the gears in the previously-mentioned aircraft engine operate very satisfactorily under high loads or high speeds (Figure 16 shows a set of the major gears). These gears were not quiet, as it was not necessary to make gears run quietly under high loads. I feel it is much more difficult to make them run quietly than just run satisfactorily. This is the problem we have in the units in the automobile today. Making them run is not enough — they must also be quiet and vibration-free. This is often a difficult problem; however, it is another subject, and a big one which cannot be included in this discussion.

INDUSTRIAL MATHEMATICS is published semi-annually by the Industrial Mathematics Society. The advance subscription price is $4.00 per annual volume of two issues. Back issues (one volume per year) are available at $3.00 per copy. Orders accompanied by check or money order should be addressed to Industrial Mathematics Society, 100 Farnsworth Street, Detroit 2, Michigan.

INDUSTRIAL MATHEMATICS contains original articles dealing with the application of mathematics in industry. Persons having such manuscripts for publication should submit them in duplicate to the Editor, INDUSTRIAL MATHEMATICS, 100 Farnsworth Street, Detroit 2, Michigan. Any questions on editorial matters should be similarly addressed.

Manuscripts should be typed double-spaced on one side of $8\frac{1}{2}$ by 11 inch paper in complete and finished form precisely as they are to appear, and sent — packed flat — to the Editor. Where possible, Figures should be numbered consecutively in arabic numerals. Tables should be numbered in arabic numerals, and both figures and tables should have captions.

Authors will receive galley proofs for correction purposes. One-hundred reprints without covers will be furnished free.

Author's institutions or companies are asked to pay a publication charge of $7.50 per printed page for articles accepted for publication.